FINNISH METEOROLOGICAL INSTITUTE
CONTRIBUTIONS

No. 165

DIAGNOSTIC STUDIES OF EXTRATROPICAL CYCLONES IN THE PRESENT AND WARMER CLIMATE

Mika Rantanen

Institute for Atmospheric and Earth System Research / Physics
Faculty of Science
University of Helsinki

Academic dissertation

To be presented, with the permission of the Faculty of Science of the University of Helsinki, for public criticism in auditorium E204, Gustaf Hällströmin katu 2, on April 24th, 2020, at 12 o'clock noon.

Helsinki 2020

Author's Address: Finnish Meteorological Institute
P.O. Box 503
FI-00101 Helsinki
mika.rantanen@fmi.fi

Supervisors: Docent Jouni Räisänen, Ph.D.
Institute for Atmospheric and Earth System Research
University of Helsinki

Docent Victoria Sinclair, Ph.D.
Institute for Atmospheric and Earth System Research
University of Helsinki

Professor Heikki Järvinen, Ph.D.
Institute for Atmospheric and Earth System Research
University of Helsinki

Reviewers: University Lecturer Jennifer Catto, Ph.D.
College of Engineering, Mathematics and Physical Sciences
University of Exeter, United Kingdom

Senior Researcher Christian Grams, Ph.D.
Institute of Meteorology and Climate Research
Karlsruhe Institute of Technology, Germany

Opponent: Professor Heini Wernli, Ph.D.
Institute for Atmospheric and Climate Science
ETH Zurich, Switzerland

ISBN 978-952-336-105-8 (paperback)
ISBN 978-952-336-106-5 (pdf)
ISSN 0782-6117

Edita Prima Oy
Helsinki 2020

ILMATIETEEN LAITOS
METEOROLOGISKA INSTITUTET
FINNISH METEOROLOGICAL INSTITUTE

Published by **Finnish Meteorological Institute**
(Erik Palménin aukio 1), P.O. Box 503
FIN-00101 Helsinki, Finland

Series title, number and report code of publication
FMI Contributions 165, FMI-CONT-165
Date: April 2020

Author
Mika Rantanen

ORCID iD
0000-0003-4279-0322

Title

Diagnostic Studies of Extratropical Cyclones in the Present and Warmer Climate

Abstract

Extratropical cyclones are among the most important weather phenomena at mid- and high latitudes. They drive the weather variability on daily basis, and the passage of a strong extratropical cyclone can occasionally cause damage for society in general and, as a specific example, forestry due to strong winds, flooding and snow load. Furthermore, extratropical cyclones are a crucial component of the atmospheric general circulation due to their ability to transport large amounts of heat and momentum.

Because of climate change, the environment in which extratropical cyclones form will change. For example, the increase of available moisture for extratropical cyclones with the warming enhances the latent heat release in the clouds, affecting thus potentially the intensity and deepening rate of extratropical cyclones, and eventually the impacts which are felt at the surface. Therefore, studying the various effects of climate change on the dynamics of extratropical cyclones is of great importance.

In this thesis, a diagnostic method was developed to analyse the physical causes of vertical motion, geopotential height tendency and relative vorticity tendency within extratropical cyclones. Information on the physical causes gives insight into the relative contribution of different moist and dry processes to the evolution of extratropical cyclones. The thesis covers studies of both an idealized, traditional type of cyclone driven by both adiabatic and diabatic dynamics, and a real-world cyclone which was transitioned from a hurricane and was found to be strongly dependent on moist processes. Information on such dynamical differences is essential during the era of changing climate, when the atmospheric moisture content is continuously increasing due to global warming.

Furthermore, the changes in the characteristics and structure of extratropical cyclones with the warming were investigated. In a model simulation in which sea surface temperatures were increased by 4 K, the precipitation associated with the cyclones increased up to 50 %, and the area of rainfall moved further away from the cyclone's centre. It was also discovered that extratropical cyclones tend to respond differently to the changes in lower-level and upper-level temperature gradient. The decrease of lower-level temperature gradient, as anticipated in northern mid-latitudes with climate change, tends to decrease the strength of extratropical cyclones in a robust way. The response of extratropical cyclones to the increase of upper-level temperature gradient seems to be, in turn, more sensitive to the presence of atmospheric moisture, which highlights the importance of mid-tropospheric latent heat release for the development of extratropical cyclones.

Publishing unit

Weather and Climate Change Impact Research

Classification (UDC)
551.515.1

Keywords: extratropical cyclones, diabatic heating, numerical models, omega equation

ISSN and series title
0782-6117
Finnish Meteorological Institute Contributions

ISBN
978-952-336-105-8 (paperback)
978-952-336-106-5 (pdf)

DOI
10.35614/isbn.9789523361065

Language
English

Pages
52

ILMATIETEEN LAITOS
METEOROLOGISKA INSTITUTET
FINNISH METEOROLOGICAL INSTITUTE

Julkaisija **Ilmatieteen laitos**
(Erik Palménin aukio 1), PL 503
00101 Helsinki

Julkaisun sarja, numero ja raporttikoodi
FMI Contributions 165, FMI-CONT-165
Päivämäärä: Huhtikuu 2020

Tekijä
Mika Rantanen

ORCID iD
0000-0003-4279-0322

Nimeke

Diagnostisia tutkimuksia keskileveysasteiden matalapaineista sekä nykyisessä että lämpimässä ilmastossa

Tiivistelmä

Liikkuvat matalapaineet ovat keski- sekä korkeiden leveysasteiden tärkeimpiä sääilmiöitä. Niiden ansiosta päivittäinen säämme on vaihtelevaa, mutta toisaalta voimakkaat matalapaineet voivat aiheuttaa vahinkoja yhteiskunnalle ja esimerkiksi metsätaloudelle myrskytuulien, tulvimisen tai lumisateiden takia. Keskileveysasteiden liikkuvat matalapaineet ovat myös tärkeä osa koko ilmakehän yleistä kiertoliikettä, koska ne kuljettavat liikemäärää ja esimerkiksi tasaavat päiväntasaajan ja korkeiden leveysasteiden suurta lämpötilaeroa.

Ilmaston lämpenemisen myötä matalapaineiden kasvuympäristö tulee muuttumaan. Esimerkiksi lämpötilan noususta johtuva ilmakehän kosteussisällön kasvu voimistaa pilvissä tapahtuvaa latentin lämmön vapautumista, mikä vaikuttaa myrskyjen voimakkuuteen, voimistumisnopeuteen ja lopulta myös niiden aiheuttamiin tuhoihin. On siis tärkeää tutkia tarkasti mitä vaikutuksia ilmastonmuutoksella on liikkuvien matalapaineiden dynamiikkaan.

Tässä tutkimuksessa kehitettiin diagnostinen työkalu jolla voitiin tutkia matalapaineissa ilmakehän pystyliikkeen sekä geopotentiaalikorkeuden ja suhteellisen pyörteisyyden muutosnopeuden fysikaalisia syitä. Tämän tiedon avulla saadaan selville miten adiabaattinen dynamiikka ja toisaalta diabaattiset prosessit vaikuttavat matalapaineiden kehitykseen, ja mikä on näiden tekijöiden keskinäinen suuruusluokka. Työssä tutkittiin sekä ideaalista, oppikirjamaista matalapainetta, sekä todellista, hurrikaanista muuntautunutta matalapainetta. Idealisoidussa tapauksessa sekä adiabaattiset että diabaattiset prosessit olivat voimakkaita, kun taas myrsky joka muuntui hurrikaanista keskileveysasteiden matalapaineeksi osoittautui vahvasti diabaattiseksi. Tällainen tieto eroavaisuuksissa myrskyjen dynamiikassa on keskeistä ilmastonmuutoksen aikakaudella, erityisesti kasvavan ilmakehän kosteussisällön takia.

Väitöskirjatyössä tutkittiin myös miten keskileveysasteiden matalapaineiden ominaisuudet ja rakenne muuttuu ilmaston lämpenemisen myötä. Tulosten mukaan neljän asteen lämpeneminen kasvatti matalapaineisiin liittyvää sateisuutta jopa 50 %. Havaittiin myös että sadealue siirtyi lämpenemisen myötä kauemmaksi myrskyn keskustasta. Lisäksi huomattiin että myrskyjen dynamiikka riippuu eri tavalla ala- ja yläilmakehän lämpötilagradienteista, jotka muuttuvat pohjoisella pallonpuoliskolla ilmaston lämmetessä. Alailmakehän lämpötilagradientin heikkeneminen vähensi matalapaineiden voimakkuutta hyvin selkeästi, kun taas yläilmakehän lämpötilagradientin kasvattaminen voimisti matalapaineita, mutta voimistumisen suuruus oli herkkä ilmakehän kosteussisällölle. Saatu tulos korostaa latentin lämmön vapautumista matalapaineiden kehityksessä.

Julkaisijayksikkö

Sään ja ilmastonmuutoksen vaikutustutkimus

Luokitus (UDK)
551.515.1

Asiasanat: keskileveysasteiden matalapaineet, diabaattinen lämmitys, numeeriset mallit, omegayhtälö

ISSN ja avainnimike
0782-6117
Finnish Meteorological Institute Contributions

ISBN
978-952-336-105-8 (nid.)
978-952-336-106-5 (pdf)

DOI
10.35614/isbn.9789523361065

Kieli
Englanti

Sivumäärä
52

Acknowledgements

I would like to first thank my supervisors, Doc. Jouni Räisänen, Doc. Victoria Sinclair and Prof. Heikki Järvinen. Jouni, your endless knowledge of atmospheric dynamics and climate change has been of great help to me. Your door has been always open for my questions and every time after our discussions I have got more faith in this work. Victoria, thanks for helping me especially in numerous technical issues, but also giving me more insight in meteorology and atmospheric sciences. Heikki, thanks for your support and mentorship during these years.

I want to thank also Dr. Juha Lento, who has been always very helpful when I have been stuck with computers. Thanks for teaching me how to do things in a "right" way in programming. Without your help this work would have never been done. I am also grateful to Prof. Heini Wernli for serving as opponent in my defence, and Dr. Jennifer Catto and Dr. Christian Grams for pre-examining this thesis.

This whole research was conducted in the Institute for Atmospheric and Earth System Research (INAR) (formerly Division of Atmospheric Sciences). I would like to thank the director of INAR, Prof. Markku Kulmala for providing me the opportunity to work in one of the world's leading atmospheric research groups. Many thanks also for Dynamic Meteorology group for giving me the wonderful working environment which was honestly the best possible place for me to carry out this research. In addition, Doctoral Programme of Atmospheric Sciences deserves special acknowledgements for financially funding this work.

Thanks for all the friends and fellow PhD students for all the fun moments, and not only during the last four years, but during the all nine years which I have been hanging out in Kumpula studying meteorology. The peer support which I have got from you has been very valuable. In addition, special thanks also to my office roommates, Meri, Madeleine and Lauri, for the all helpful discussions which we have had.

Finally, I would like to express my deepest gratitude to the love of my life, Jessica, who has been raising our two daughters, Olivia and Ellen, at home when I have been spending long days at work. I want to thank you for all of your support and sacrifices you have made for me throughout these years.

Mika Rantanen
Lahti, February 2020

Contents

List of publications

This thesis consists of an introductory review, followed by four research articles. In the introductory part, these papers are cited according to their roman numerals. **Paper I** is reprinted under the Creative Commons Attribution 3.0 license, **Paper II** is printed by permission from Springer Nature (licence number 4750131311239), **Paper III** is reprinted under the Creative Commons Attribution-NonCommercial 4.0 License and **Paper IV** is reprinted under the Creative Commons Attribution 4.0 license.

I **Rantanen, M.**, Räisänen, J., Lento, J., Stepanyuk, O., Räty, O., Sinclair, V. A., and Järvinen, H. (2017). OZO v.1.0: software for solving a generalised omega equation and the Zwack-Okossi height tendency equation using WRF model output, *Geoscientific Model Development*, 10, 827-841, doi:10.5194/gmd-10-827-2017

II **Rantanen, M.**, Räisänen, J., Sinclair, V.A. and Järvinen, H. (2019). Sensitivity of idealised baroclinic waves to mean atmospheric temperature and meridional temperature gradient changes, *Climate Dynamics* 52: 2703. doi:10.1007/s00382-018-4283-3

III **Rantanen, M.**, Räisänen, J., Sinclair, V.A. and Järvinen, H. (2020). The extratropical transition of Hurricane Ophelia (2017) as diagnosed with a generalized omega equation and vorticity equation, *Tellus A: Dynamic Meteorology and Oceanography*, 72, 1-26 doi:10.1080/16000870.2020.1721215

IV Sinclair, V.A., **Rantanen, M.**, Haapanala, P., Räisänen, J. and Järvinen, H. (2020). The structure of extratropical cyclones in warmer climates, *Weather and Climate Dynamics*, 1, 1-25 doi:10.5194/wcd-1-1-2020

1 Introduction

1.1 What is an extratropical cyclone?

Extratropical cyclones (hereafter ETCs), often called also as mid-latitude cyclones, are weather systems ranging in size from several hundreds of kilometres to a few thousand kilometres. They form due to atmospheric baroclinicity (i.e. temperature difference in north-south direction), and are thus most abundant and strongest in the winter season when the temperature differences between low- and high latitudes are greatest. ETCs are the main cause of weather variability at mid- and high latitudes. They bring precipitation and winds, and the strongest ETCs can cause societal damage (e.g. Wernli et al., 2002; Liberato et al., 2011, 2013), such as traffic disruption or power outages. The low-level airflows associated with ETCs can form so called atmospheric rivers (Dacre et al., 2019), which can lead to serious flooding for example in UK (Lavers et al., 2011) and the west coast of USA (Ralph et al., 2006).

Because ETCs typically form in the area of strong baroclinicity, they are associated with fronts and thus their appearance looks asymmetric. This is one of the main characteristics distinguishing them from tropical cyclones, which are usually more symmetric by their appearance. In addition, tropical cyclones develop through latent heat release in deep convective clouds and thus their occurrence is restricted to lower latitudes where the sea surface temperatures are higher. Extratropical cyclogenesis instead, tends to occur at mid- and high latitudes, in the Northern Hemisphere most frequently in the so-called North Pacific and North Atlantic storm tracks (Wernli and Schwierz, 2006). Furthermore, tropical cyclones can sometimes curve poleward, enter mid-latitudes and transform into ETCs. These post-tropical storms can cause high-impact weather downstream via amplification of the mid-latitude flow (e.g. Grams and Blumer, 2015; Grams and Archambault, 2016).

ETCs have an important role in atmospheric general circulation. They transport both sensible heat (warm air) and latent heat (moisture) from lower latitudes towards the poles, and at mid-latitudes, they are actually more efficient meridional heat transporters than ocean currents (e.g. Hartmann, 2015). Therefore, without ETCs, the temperature difference between the tropics and poles would be considerably higher. Furthermore, ETCs participate to the energy cycle of our climate system by converting the atmospheric available potential energy to kinetic energy (Lorenz, 1955), which

can be felt at the surface as winds.

In summary, although ETCs are often associated with undesirable weather, they are a crucial part of our climate system. Moreover, due to climate change, the structure and dynamics, and thus potentially the impacts of ETCs on our society may change. For all these reasons, studying the dynamics of ETCs in our changing climate is of great interest.

1.2 Different diagnostic methods

Various studies during the past century have contributed to understanding the role of different physical processes in the development of ETCs (Schultz et al., 2019). The baroclinic theory and the adiabatic processes thereof became well-known during the mid-20th century (Charney, 1947; Eady, 1949). Since then, the role of latent heat release due to formation of clouds and precipitation in baroclinic disturbances has gained attention among the researchers (e.g. Tracton, 1973; Kuo et al., 1991; Stoelinga, 1996). Nowadays it is well understood that diabatic processes can considerably affect the strength of ETCs (e.g. Ahmadi-Givi et al., 2004; Büeler and Pfahl, 2017), especially in warm season (Martínez-Alvarado et al., 2016) and marine cyclones (Roebber and Schumann, 2011).

Diagnostic methods to identify the contributions of various adiabatic and diabatic processes to the development of ETCs have been developed during the years. The key variable to diagnose the effect of diabatic heating is potential vorticity (PV; Rossby, 1939; Ertel, 1942) due to its conservativity in adiabatic and frictionless conditions. Hoskins et al. (1985) later established the use of PV in modern atmospheric dynamics. Because PV can be only modified by diabatic and frictional processes, the appliance of PV inversion techniques allows to determine explicitly the contribution of diabatic processes to the circulation and intensity of ETCs (Davis and Emanuel, 1991; Stoelinga, 1996).

Because the low-level PV anomalies associated with ETCs are strongly coupled to cyclone intensity, diagnostic methods using PV alone are also useful to explain the role of latent heating especially in explosive cyclogenesis. Using the PV framework, Büeler and Pfahl (2017) developed a diagnostic approach to systematically quantify the contribution of latent heating to cyclone intensification. They applied the method

further to surrogate climate change simulations (Büeler and Pfahl, 2019) and found that enhanced diabatic heating was able to largely explain the varying increase in intensity and impacts of most of the studied cyclones. The PV framework was also employed by Chagnon et al. (2013) and Martínez-Alvarado et al. (2016), who used PV tracers to investigate the effect of diabatic processes on the evolution of ETCs. The use of tracers allowed to identify which diabatic processes in the clouds (such as evaporation and condensation) were responsible for the generation of PV anomalies within ETC.

In addition to the PV framework, the roles of different physical processes on ETC evolution can be quantified with various other techniques. Fink et al. (2012) diagnosed the influence of diabatic processes on explosive cyclogenesis using a novel version of surface pressure tendency equation (Knippertz and Fink, 2008; Knippertz et al., 2009). They applied the tool for five selected European windstorms (Storms Lothar, Martin, Klaus, Kyrill and Xynthia) and discovered that Kyrill and Martin were more baroclinically-driven storms than Lothar, Klaus and Xynthia. A more systematic analysis with the same diagnostic tool was performed later in Pirret et al. (2017), who examined 58 different European windstorms using ERA-Interim reanalysis data. According to their results, the contribution of diabatic processes varied considerably from case to case, with baroclinic processes still being the dominant forcing in the majority of storms.

The role of physical forcing mechanisms in the relative vorticity budgets of North Atlantic ETCs was studied by Azad and Sorteberg (2014a,b). They employed a generalized omega equation to decompose the vertical motion into contributions from different forcing terms: vorticity advection, temperature advection, diabatic heating, ageostrophic vorticity tendency and friction (see Section 2.2). They followed mainly the method presented earlier in Pagé et al. (2007), Räisänen (1995) and Pauley and Nieman (1992). After this, the vorticity tendency budget was partitioned into the same components representing the earlier listed physical processes, analogously with the vertical motion, and similarly as in Räisänen (1997). However, while Räisänen (1997) applied the nonlinear balance equation to further convert the vorticity tendencies to geopotential height tendencies, Azad and Sorteberg (2014a,b) relied purely on vorticity diagnostics calculated with the Zwack-Okossi equation (Zwack and Okossi, 1986; Lupo et al., 1992). Besides the papers by Azad and Sorteberg (2014a,b), the Zwack-Okossi equation has been applied successfully in numerous other diagnostic studies on ETC dynamics (e.g. Yoshida and Asuma, 2004; Azad and Sorteberg, 2009; Kuwano-Yoshida and Enomoto, 2013; Fu et al., 2018).

In conclusion, this literature review reveals that several diagnostic equations have been developed to investigate ETCs. The common denominator of these methods is that they all aim to diagnose the role of different adiabatic and diabatic processes in the life cycle of ETCs. However, the used variable can be PV tendency (e.g. Chagnon et al., 2013; Büeler and Pfahl, 2017), surface pressure tendency (e.g. Fink et al., 2012; Pirret et al., 2017), geopotential height tendency (**Paper I**, Räisänen, 1997) or vorticity tendency (e.g. **Paper III**, Azad and Sorteberg, 2014a).

Each of the listed methodologies have their own advantages and disadvantages, and depending on the properties of the used dataset and the specific aim of the research, any of these methods can be beneficial. For example, if one wants to study specifically the impact of free-tropospheric moist processes to ETCs, applying PV diagnostic could be useful because in the free troposphere PV can only be modified by diabatic heating, which largely consists of the latent heat release in the clouds. Instead, the benefit of applying the vorticity- or geopotential height tendency methodology (**Paper I**, **Paper III**) is that they allow to decompose also the adiabatic processes into the contributions from vorticity advection, thermal advection, and ageostrophic vorticity tendency. This would not be possible using PV tendency alone.

1.3 Implications of warmer climate on extratropical cyclones

The ongoing climate change can affect the behaviour of ETCs in several different ways: (1) by increasing the atmospheric moisture content due to increasing temperatures (Hartmann et al., 2013); (2) by decreasing the lower level meridional temperature gradient due to larger warming trend in Arctic regions (known as Arctic amplification, e.g. Serreze et al., 2009) than elsewhere in the globe; and (3) by increasing the upper level meridional temperature gradient due to enhanced warming in the tropical upper troposphere (e.g. Allen and Sherwood, 2008) and cooling in the polar lower stratosphere (e.g. Thompson and Solomon, 2005). The changes (2) and (3) constitute a balanced tug-of-war between two competing effects for the strength of the jet stream, as verified recently by reanalysis datasets (Lee et al., 2019). Because these changes (1)-(3) are occurring simultaneously in the atmosphere, and given the nonlinear responses of ETCs to these changes, it is not surprising that confident future projections of midlatitude storm tracks remain challenging. Accordingly, The Intergovernmental Panel on Climate Change (IPCC) states in its 5th assessment report that "Substantial uncertainty and

thus low confidence remains in projecting changes in NH winter storm tracks, especially for the North Atlantic basin." (Collins et al., 2013).

The latest research on the implications of climate change on the structure and dynamics of ETCs were recently brought together in a review paper by Catto et al. (2019). According to the review, the most robust outcome in the recent studies is that in a warmer climate, the precipitation associated with ETCs will increase (e.g. **Paper IV**, Yettella and Kay, 2017; Hawcroft et al., 2018). What remains still unclear is how the enhanced latent heating associated with increased precipitation will materialize in the intensity of ETCs. This research question is particularly challenging because there are different ways to define the intensity of ETCs, such as surface winds, eddy kinetic energy, minimum surface pressure or the deepening rate (Catto et al., 2019).

Numerical experiments performed with idealized climate change simulations have provided insights on the effect of increasing atmospheric moisture content on ETC intensity (e.g. **Paper II**, **Paper IV**, Booth et al., 2013; Kirshbaum et al., 2018; Tierney et al., 2018). One common aspect seems to be that the eddy kinetic energy is very close to its maximum with present-day climate conditions and is expected to decrease with further warming (**Paper III**, O'Gorman and Schneider, 2008; Pfahl et al., 2015; Kirshbaum et al., 2018; Tierney et al., 2018). One explanation for this could be structural changes in ETCs, such as worse phasing between the warm-frontal ascent and the buoyancy in the warm sector, as found in Kirshbaum et al. (2018) and confirmed later in **Paper III**.

Climate models in Coupled Model Intercomparison Project 5 (CMIP5) predict that the number of strong cyclones would decrease in the North Atlantic by 8 % $\pm$ 3 % (in winter) or 6 % $\pm$ 3 % (in summer) in RCP4.5 scenario by the end of 21st century (Zappa et al., 2013b). Furthermore, under the high-emission RCP8.5 scenario, the extreme winds associated ETCs are projected to decrease 17 % for the entire Northern Hemisphere by the end of the 21st century (Chang, 2018). However, the sign of change is the opposite in the Southern Hemisphere, where CMIP5 models project an increase in the number of strong cyclones (Chang et al., 2012). The deepening rate of ETCs in warmer climates does not seem to change significantly in idealized simulations (Pfahl et al., 2015) or in CMIP5 models in the Northern Hemisphere (Seiler and Zwiers, 2016). However, according to the results of **Paper IV**, and consistent with the Southern Hemisphere CMIP5 projections (Chang et al., 2012), the deepening rate of particularly strong ETCs may increase with the warming.

There is evidence that CMIP5 models have systematic biases in the number and intensity of North Atlantic ETCs (Zappa et al., 2013a; Pithan et al., 2016). Furthermore, it has been shown that diabatic heating in the clouds is sensitive to the model resolution (Willison et al., 2013, 2015). Thus, more research on this subject is clearly needed, especially with high-resolution models using state-of-the-art physics parametrizations. In their review paper on the future of ETCs Catto et al. (2019) emphasize that "Future research could focus on bridging the gap between idealized models and complex climate models, as well as better understanding of the regional impacts of future changes in extratropical cyclones."

1.4 Aims of the thesis

The general aim of this thesis is to increase the understanding on how different atmospheric physical processes can affect the intensity and structure of ETCs, both in present-day climate conditions and in a warmer climate. This aim has been addressed in four research articles, with the following more specific research questions:

1. How much do different adiabatic and diabatic processes contribute to the evolution of ETCs? For this purpose, a diagnostic tool has been developed, and the contributions of different adiabatic and diabatic processes were analysed quantitatively using idealized and real-world case studies in **Paper I** and **III**.

2. How sensitive are ETCs to different aspects of changes in the mean temperature distribution, which are anticipated with climate change in the Northern Hemisphere? This specific aim was addressed in **Paper II** with model simulations in which the large-scale temperature environment experienced by a developing ETC was altered. The simulations were compared to a control run where no changes were performed.

3. Which structural changes are expected to occur in ETCs in a warmer climate, if any, and which physical processes are responsible for these changes? This final aim was investigated with 10-year long simulations with global atmospheric model in **Paper IV**. The structural changes were identified with a cyclone-compositing method.

2 Diagnostic methods and model simulations

In this section, the equations and the model simulations used in this thesis are presented. The diagnostic tool employed in **Paper I** and **III** is based on the decomposition of vertical motion into its physical causes. The method for the decomposition is presented first, in Section 2.1. The strengthening and weakening rate of ETCs was studied using time tendencies of both geopotential height and relative vorticity. The decomposition of these variables is presented in Section 2.2. In addition, the validation of both diagnostic methods is demonstrated in Section 2.3. Then, the basic concept of the energy cycle in the atmosphere and its relation to ETCs is expressed in Section 2.4, and finally, the used numerical weather models and the experiments are briefly introduced in Section 2.5.

2.1 The decomposition of vertical motion

Albeit being often orders of magnitude weaker than the horizontal wind, the vertical wind is a vital part of the atmospheric general circulation. In ETCs, vertical motions are tightly linked to the development of the system: rising motions generate low-level cyclonic vorticity, and when occurring near the cyclone centre, they act to increase the intensity of the system. Furthermore, upward motions lead to adiabatic cooling and consequently to condensation of water vapour. Thus, upward motions are an essential ingredient of the precipitation and latent heat release in ETCs. Moreover, the ascent of warm air and descent of cold air in the eddies convert the available potential energy to kinetic energy, and hence influence the whole energy cycle of the atmosphere. For these reasons, understanding the physical and dynamical causes of the vertical motions in the ETCs is of great importance.

A practical and broadly used way to examine the causes of atmospheric vertical motion is to apply the omega equation. Various forms of the omega equation exist, ranging from the simplest quasi-geostrophic (QG) omega equation to the most complex, generalized version of the omega equation. In this thesis, the main diagnostic tool is based on the generalized omega equation, but two simpler forms of omega equations have also been utilized.

The QG omega equation, which is briefly used in **Paper I**, is presented first:

$$L_{QG}(\omega) = F_{V(QG)} + F_{T(QG)} \tag{1}$$

where

$$L_{QG}(\omega) = \sigma_0\,(p)\,\nabla^2\omega + f^2\frac{\partial^2\omega}{\partial p^2} \tag{2}$$

and the two right-hand-side (RHS) terms are

$$F_{V(QG)} = f\frac{\partial}{\partial p}\left[\vec{V}_g \cdot \vec{\nabla}\left(\zeta_g + f\right)\right] \tag{3}$$

$$F_{T(QG)} = \frac{R}{p}\nabla^2\left(\vec{V}_g \cdot \vec{\nabla}T\right). \tag{4}$$

The explanations of all mathematical symbols are listed in Table 1. The QG omega equation tells that rising motion in the atmosphere occurs if the cyclonic vorticity advection increases upwards (Eq. 3) or if there is advection of warm air (Eq. 4). The opposite is true for the sinking motion.

The main advantage of the QG omega equation is that it is computationally light to solve and gives still a relatively good approximation of the mid-tropospheric vertical motion decomposed into the contributions from vorticity advection and thermal advection. However, for detailed analysis of the causes of vertical motion, especially in systems which are strongly diabatically-driven, the QG approximations become inevitably problematic. To avoid the QG approximations, one can derive a generalized omega equation directly from the primitive equations (e.g. Räisänen, 1995). Hence, the generalized omega equation does not involve any simplifying assumptions except the hydrostatic balance, which is implicitly assumed when isobaric coordinates are used.

In **Papers I** and **III**, we used the following formulation of the generalized omega equation:

$$L(\omega) = F_V + F_T + F_F + F_Q + F_A \tag{5}$$

where

$$L(\omega) = \nabla^2(\sigma\omega) + f(\zeta + f)\frac{\partial^2\omega}{\partial p^2} - f\frac{\partial^2\zeta}{\partial p^2}\omega + f\frac{\partial}{\partial p}\left[\vec{k}\cdot\left(\frac{\partial\vec{V}}{\partial p}\times\nabla\omega\right)\right] \tag{6}$$

and the RHS terms are

$$F_V = f\frac{\partial}{\partial p}\left[\vec{V}\cdot\nabla\left(\zeta + f\right)\right], \tag{7}$$

$$F_T = \frac{R}{p}\nabla^2\left(\vec{V}\cdot\nabla T\right), \tag{8}$$

$$F_F = -f\frac{\partial}{\partial p}\left[\vec{k}\cdot\left(\nabla\times\vec{F}\right)\right], \tag{9}$$

$$F_Q = -\frac{R}{c_p p}\nabla^2 Q, \tag{10}$$

$$F_A = f\frac{\partial}{\partial p}\left(\frac{\partial\zeta}{\partial t}\right) + \frac{R}{p}\nabla^2\left(\frac{\partial T}{\partial t}\right). \tag{11}$$

The RHS forcing terms represent the effects of vorticity advection (F_V, Eq. 7), thermal advection (F_T, Eq. 8), friction (F_F, Eq. 9), diabatic heating (F_Q, Eq. 10), and an imbalance between vorticity tendency and temperature tendency (hereafter imbalance term, F_A, Eq. 11).

Finally, in **Paper IV**, an intermediate form of the omega equation, which employs the main forcing terms of the generalized omega equation (vorticity advection, thermal advection and diabatic heating), but the simplified LHS operators from the QG omega equation (Eq. 2), was used:

$$\sigma_0(p)\nabla^2\omega + f^2\frac{\partial^2\omega}{\partial p^2} = f\frac{\partial}{\partial p}\left(\vec{V}\cdot\nabla\left(\zeta+f\right)\right) + \frac{R}{p}\nabla^2\left(\vec{V}\cdot\nabla T\right) - \frac{R}{c_p p}\nabla^2 Q. \tag{12}$$

Here the friction term was neglected as is was assumed to be small in an aquaplanet configuration where only ocean exists. In addition, as the horizontal resolution was rather coarse (around 125 km), the imbalance term in synoptic-scale systems can be expected to be relatively small and thus could be ignored.

With homogenous boundary conditions (ω=0 at the lower and upper boundary of the atmosphere), the vertical motion contributions of the individual RHS terms can be solved separately because the LHS operators (Eq. 2 and 6) are linear with respect to ω. As a result, the total vertical motion is decomposed into contributions from different physical processes. For the QG omega equation, this means that the total vertical motion consists of two omega terms:

$$\omega_{QG} = \omega_{V(QG)} + \omega_{T(QG)} \tag{13}$$

Here $\omega_{V(QG)}$ means vertical motion that is due to the vorticity advection term and $\omega_{T(QG)}$ vertical motion that is due to the thermal advection term.

For the generalized omega equation (Eq. 5), the calculated total vertical motion field consists of five omega terms:

$$\omega = \omega_V + \omega_T + \omega_F + \omega_Q + \omega_A \tag{14}$$

In this case, the different ω-terms on the RHS mean vertical motion due to vorticity advection (ω_V), thermal advection (ω_T), friction (ω_F), diabatic heating (ω_Q) and imbalance term (ω_A), analogously to Eq. 5.

All the data needed for solving the equations were obtained directly from the model output, which was vertically interpolated to pressure coordinates. In **Paper I**, we solved the omega equations (both QG and generalized) on a Cartesian grid with a so-called multigrid algorithm. In **Paper III**, the generalized omega equation was applied in spherical coordinates, which meant that we could not utilize the same solver as in **Paper I**. Thus, the solving was performed with Portable, Extensible Toolkit for Scientific Computation (PETSc) differential equation solvers, which allowed us to use parallel computing with supercomputer resources. Finally, the intermediate form of omega equation used in **Paper IV** was solved in spectral space, using the method from Räisänen (1995). In summary, in all of the papers slightly different solving methods for the omega equation were applied, due to the fact that the LHS operators and the used coordinate system varied between the studies.

The generalized omega equation has been used only in a few earlier studies which have aimed to diagnose the different forcing terms affecting ETCs. The method used here builds on Räisänen (1997), nearly similarly as has been done in Caron et al. (2006) and Azad and Sorteberg (2014a,b). However, some technical differences between the methodologies exists. For example, Caron et al. (2006) and Azad and Sorteberg (2014a,b) calculate the frictional tendencies $\vec{F}$ assuming balance between pressure gradient and the frictional and Coriolis forces in the lowest 150 hPa (Caron et al., 2006) or below 850 hPa (Azad and Sorteberg, 2014a,b). In addition, in these studies the diabatic heating rate Q was estimated using the total surface precipitation flux and positive diabatic residuals estimated by the thermodynamic equation. In **Papers I, III** and **IV**, however, $\vec{F}$ and Q were obtained directly from the model output, which simplifies the workflow and increases the numerical accuracy of these tendencies.

Table 1: List of mathematical symbols.

$c_p = 1004$ J kg^{-1}	specific heat of dry air at constant volume
f	Coriolis parameter
F	forcing in the omega equation
$\vec{F}$	friction force per unit mass
$g = 9.81$ m s^{-2}	gravitational acceleration
$\vec{k}$	unit vector along the vertical axis
L	linear operator on the left-hand-side of the omega equation
p	pressure
Q	diabatic heating rate per mass
$R = 287$ J kg^{-1}	gas constant of dry air
$S = -T\frac{\partial ln\theta}{\partial p}$	stability parameter in pressure coordinates
t	time
T	temperature
$\vec{V}$	horizontal wind vector
$\vec{V_g}$	geostrophic wind vector
$\sigma = -\frac{RT}{p\theta}\frac{\partial \theta}{\partial p}$	hydrostatic stability
σ_0	isobaric mean of hydrostatic stability
ζ	vertical component of relative vorticity
ζ_g	relative vorticity of geostrophic wind
ζ_{ag}	relative vorticity of ageostrophic wind
$\omega = \frac{dp}{dt}$	isobaric vertical motion
∇	horizontal nabla operator
∇^2	horizontal laplacian operator

2.2 The decomposition of geopotential height tendency and vorticity tendency

In addition to atmospheric vertical motion, the tendencies of geopotential height and relative vorticity are key variables in studying ETCs because these variables are directly linked to the strengthening or weakening rate of ETCs. With constant Coriolis parameter, the relation between geopotential height tendency and geostrophic vorticity

tendency is as follows:

$$\frac{\partial \zeta_g}{\partial t} = \frac{g}{f}\nabla^2 \frac{\partial Z}{\partial t} \tag{15}$$

Thus, in the Northern Hemisphere, the first order approximation is that positive height tendency means negative vorticity tendency and vice versa.

In **Paper I**, we used the so-called Zwack-Okossi equation (Zwack and Okossi, 1986; Lupo and Smith, 1998)

$$\frac{\partial \zeta_g}{\partial t}(p_L) = \frac{1}{p_s - p_t}\left[\int_{p_t}^{p_s}\left(\frac{\partial \zeta}{\partial t} - \frac{\partial \zeta_{ag}}{\partial t}\right)dp - \frac{R}{f}\int_{p_t}^{p_s}\left(\int_{p}^{p_L}\nabla^2 \frac{\partial T}{\partial t}\frac{dp}{p}\right)dp\right] \tag{16}$$

to decompose the tendency of geostrophic vorticity into components of various forcing terms. Here p_L is the level for which the tendency is calculated, and p_s and p_t are the lower and the upper boundaries of the model domain. The vorticity tendency $\frac{\partial \zeta}{\partial t}$ in the first term of Eq. 16 was calculated using the vorticity equation

$$\frac{\partial \zeta}{\partial t} = -\vec{V}\cdot\nabla(\zeta + f) - \omega\frac{\partial \zeta}{\partial p} + (\zeta + f)\frac{\partial \omega}{\partial p} + \vec{k}\cdot\left(\frac{\partial \vec{V}}{\partial p}\times\nabla\omega\right) + \vec{k}\cdot\nabla\times F, \tag{17}$$

and temperature tendency $\frac{\partial T}{\partial t}$ in the second term of Eq. 16 was calculated using the thermodynamic equation:

$$\frac{\partial T}{\partial t} = -\vec{V}\cdot\nabla T + S\omega + \frac{Q}{c_p} \tag{18}$$

The ageostrophic vorticity tendency was estimated using central time differences

$$\frac{\partial \zeta_{ag}}{\partial t} \approx \frac{\Delta(\zeta - \zeta_g)}{2\Delta t}. \tag{19}$$

with $\Delta t = 1800\ s$.

When substituting the vorticity equation (Eq. 17) and the thermodynamic equation (Eq. 18) into Eq. 16, utilizing the different omega terms from Eq. 14, and finally combining the result with Eq. 15, the different geopotential height tendency terms can be derived, analogously with the vertical motion:

$$\frac{\partial Z}{\partial t} = \left(\frac{\partial Z}{\partial t}\right)_V + \left(\frac{\partial Z}{\partial t}\right)_T + \left(\frac{\partial Z}{\partial t}\right)_F + \left(\frac{\partial Z}{\partial t}\right)_Q + \left(\frac{\partial Z}{\partial t}\right)_A. \tag{20}$$

Here the RHS terms mean geopotential height tendencies that are due to vorticity advection, thermal advection, friction, diabatic heating and imbalance term, respectively. See **Paper I** for the full forms of the RHS terms of Eq. 20.

In **Paper III**, the cyclone development was analysed using vorticity tendencies. The decomposition was similar to that in Räisänen (1995):

$$\frac{\partial \zeta}{\partial t} = \left(\frac{\partial \zeta}{\partial t}\right)_V + \left(\frac{\partial \zeta}{\partial t}\right)_T + \left(\frac{\partial \zeta}{\partial t}\right)_F + \left(\frac{\partial \zeta}{\partial t}\right)_Q + \left(\frac{\partial \zeta}{\partial t}\right)_A . \tag{21}$$

where

$$\left(\frac{\partial \zeta}{\partial t}\right)_V = -\vec{V} \cdot \nabla(\zeta + f) - \omega_V \frac{\partial \zeta}{\partial p} + (\zeta + f)\frac{\partial \omega_V}{\partial p} + \vec{k} \cdot \left(\frac{\partial \vec{V}}{\partial p} \times \nabla \omega_V\right), \tag{22}$$

$$\left(\frac{\partial \zeta}{\partial t}\right)_F = \vec{k} \cdot \nabla \times \vec{F} - \omega_F \frac{\partial \zeta}{\partial p} + (\zeta + f)\frac{\partial \omega_F}{\partial p} + \vec{k} \cdot \left(\frac{\partial \vec{V}}{\partial p} \times \nabla \omega_F\right), \tag{23}$$

and

$$\left(\frac{\partial \zeta}{\partial t}\right)_X = -\omega_X \frac{\partial \zeta}{\partial p} + (\zeta + f)\frac{\partial \omega_X}{\partial p} + \vec{k} \cdot \left(\frac{\partial \vec{V}}{\partial p} \times \nabla \omega_X\right), \; X = T, Q, A \tag{24}$$

Similarly as in Eq. 20, the RHS terms of Eq. 21 describe the vorticity tendencies due to vorticity advection, thermal advection, diabatic heating, friction and the imbalance term, respectively.

2.3 Model simulations

The results presented in this thesis are based on simulations performed with numerical weather models. In **Paper I** and **II**, we used the Weather Research and Forecasting (WRF) model (Shamarock et al., 2008) with its baroclinic wave channel mode. In **Paper III** and **IV**, the Open Integrated Forecast System (OpenIFS) model was used. Short technical information about these two models and the model simulations is presented next.

2.3.1 Baroclinic wave simulations

The WRF model can be used for simulating atmospheric conditions using either real data or idealised cases. In **Paper I** and **II**, an idealised moist baroclinic wave simulation was used. This baroclinic wave configuration is a highly controlled model set-up, which simulates the evolution of only one ETC within a baroclinically unstable jet in the

Northern Hemisphere under constant Coriolis parameter. In both **Paper I** and **II**, the value of the Coriolis parameter was set to 10^{-4}, which corresponds to the latitude of 43°N. The evolution of the baroclinic wave was triggered by inserting a 1-K temperature perturbation to the mid-tropospheric temperature field.

The boundaries of the model domain were periodic in east-west direction. This means that we did not need to have an exceedingly wide model domain in order to simulate the whole life cycle of the eastward-propagating cyclone. In the north-south direction, symmetric boundaries were used. In **Paper I**, the size of the model domain was 4000 km x 8000 km x 16 km, in the x, y and z directions, respectively. In **Paper II**, the length was 5000 km in the x direction with the other directions the same as in **Paper I**.

The model simulations in **Papers I and II** featured full physics schemes, except that the radiation scheme was switched off. The choice of leaving radiation off is a widely used procedure in baroclinic wave simulations (e.g. in Booth et al., 2013; Kirshbaum et al., 2018; Tierney et al., 2018) in order to help the interpretation of diabatic heating, as the latent heat release becomes the only major source of diabatic heating in the free atmosphere. See **Paper I** and **II** for detailed descriptions of the used model parametrizations schemes.

The main aim in **Paper I** was to document the diagnostic software and test its applicability for baroclinic wave simulations. For this reason, the simulation used to demonstrate the usability of the software was based largely on the standard baroclinic wave simulation which comes along with the WRF model package. The horizontal grid spacing was 25 km and there were 64 sigma levels in the vertical dimension.

In **Paper II**, we investigated the changes of cyclone energetics using three scenarios which are expected to occur with climate change in the Northern Hemisphere: (1) uniform increase of temperature; (2) decrease of the lower level meridional temperature gradient; and (3) increase of the upper level temperature gradient. The uniform increase of temperature in (1) was performed by raising the atmospheric temperature stepwise by 2, 4 and 6 K in the initial state of the model run. In (2), we decreased the low-level temperature gradient by warming the southern part of the domain and cooling the northern part of the domain by 2, 4 and 6 K. This acted to decrease the gradient by 4, 8, and 12 K, respectively. A similar procedure was done in (3), but to the opposite direction and at upper levels. More details about the experiments are

presented in **Paper II**.

Even though the changes (1) - (3) are occurring simultaneously in the real world, their effects to the intensity and energy cycle of the simulated ETC were studied separately. Moreover, we conducted the simulations first without moisture in the atmosphere, and then with more realistic, moist environment. The justification for this practise was that we wanted to identify the underlying adiabatic mechanisms which drive the response of ETCs to different types of changes in environmental temperature.

2.3.2 Global model simulations

OpenIFS is a global model developed by the European Centre for Medium-Range Weather Forecasts (ECMWF). OpenIFS has exactly same dynamical core and the physics parametrizations as the full Integrated Forecast System (IFS) model, which is used operationally for weather forecasting at ECMWF. OpenIFS does not have data assimilation capacity, but the model can be used for research purposes with externally generated initial conditions. OpenIFS is tailored to simulate real world cases, such as Storm Ophelia in **Paper III**, but it is also possible to employ OpenIFS with idealised set-up, such as the aquaplanet configuration in **Paper IV**. The version of OpenIFS used in this thesis was Cy40r1, documentation of which is available in ECMWF (2014).

In **Paper III**, we applied OpenIFS for simulating the extratropical transition of Hurricane Ophelia. The spectral resolution of the model was T639, which corresponds to approximately 31 km grid spacing at equator. Vertically there were 137 levels. The initial conditions were generated from ECMWF operational analyses, and a 6-day model simulation was initialized at 12 UTC 13 October 2017. The chosen initialization time was a compromise between the accuracy of the forecast and the length of the tropical phase of Ophelia in the simulation.

The model simulations in **Paper IV** were performed in an aquaplanet mode, a special configuration in which the surface of the Earth is all ocean. The sea surface temperatures (SST) were zonally uniform and symmetric about the equator. The atmosphere was initialized from a randomly selected real analysis from ECMWF. Two model simulations were carried out: the control simulation in which SSTs resembled the real, observed values, and a perturbed experiment in which SSTs were uniformly warmed by 4 K everywhere. These two experiments were run for 11 years, but the first year in

both experiments was discarded to make sure that the model had reached a balanced state. The experiments featured the diurnal cycle but no seasonal cycle; the incoming solar radiation was fixed to its equinoctial value. The model was run at T159 resolution (corresponding to approximately 125 km grid spacing) and with 60 model levels.

In both **Papers III** and **IV**, an objective cyclone tracking algorithm, TRACK (Hodges, 1994, 1995) was applied. TRACK was used to identify ETCs as localised maximum of 850-hPa relative vorticity truncated to T42 (**Paper IV**) or T63 (**Paper III**) resolution. In **Paper III**, TRACK was used to objectively determine the track of Ophelia in the OpenIFS simulation, and to calculate various diagnostic variables following the centre of the storm. In **Paper IV**, TRACK was applied to identify all ETCs occurring at 20°N - 90°N, travelling at least 1000 km and lasting at least for two days. These criteria were applied in order to avoid including tropical, stationary and mesoscale systems to the analysis.

After identifying the cyclone tracks in **Paper IV**, the structural changes were investigated with composite averages of the cyclones. These composites were created from the 200 strongest ETCs in both the control and the warm experiments. The method of creating the composites was the same as in Catto et al. (2010) and Dacre et al. (2012), and is briefly explained as follows. First, the tracks of the 200 strongest cyclones were identified from the model output data. Then, along the tracks, relevant meteorological variables were interpolated to a spherical grid centered on the cyclone centre, and after this, the tracks were rotated so that all the cyclones were travelling to the same direction. Finally, before taking the composite averages, the life cycles of the storms were offset with respect to the time of maximum intensity. With these procedures, we avoided the smoothing errors which would arise from averaging together cyclones which were travelling to the opposite directions, or were in a totally different stage in their life cycle.

2.4 Validation of the diagnostic methods

2.4.1 Vertical motion

In order to validate the diagnostic method, the vertical motion calculated by the omega equation was compared to the model-resolved vertical motion in **Paper I**, **III** and **IV**. As seen from Fig. 1d, the QG omega equation gives a reasonably good estimate of

the areas of strongest upward and downward motion, but many small-scale details are missing compared to ω from the WRF model (Fig. 1b). For this reason, the time-averaged correlation between the QG omega equation and ω from WRF in the simulation represented in **Paper I** was only 0.53 at 700 hPa (not shown). In the upper troposphere, where the effect of neglected terms (diabatic heating and friction) is smaller, the correlation was slightly better, being around 0.65. The intermediate form of omega equation used in **Paper IV** was found to describe vertical motion clearly better than the QG omega equation. In the latitude band of 30-60°N we documented correlation coefficients of 0.84 at 700 hPa and over 0.9 at 500 hPa (not shown).

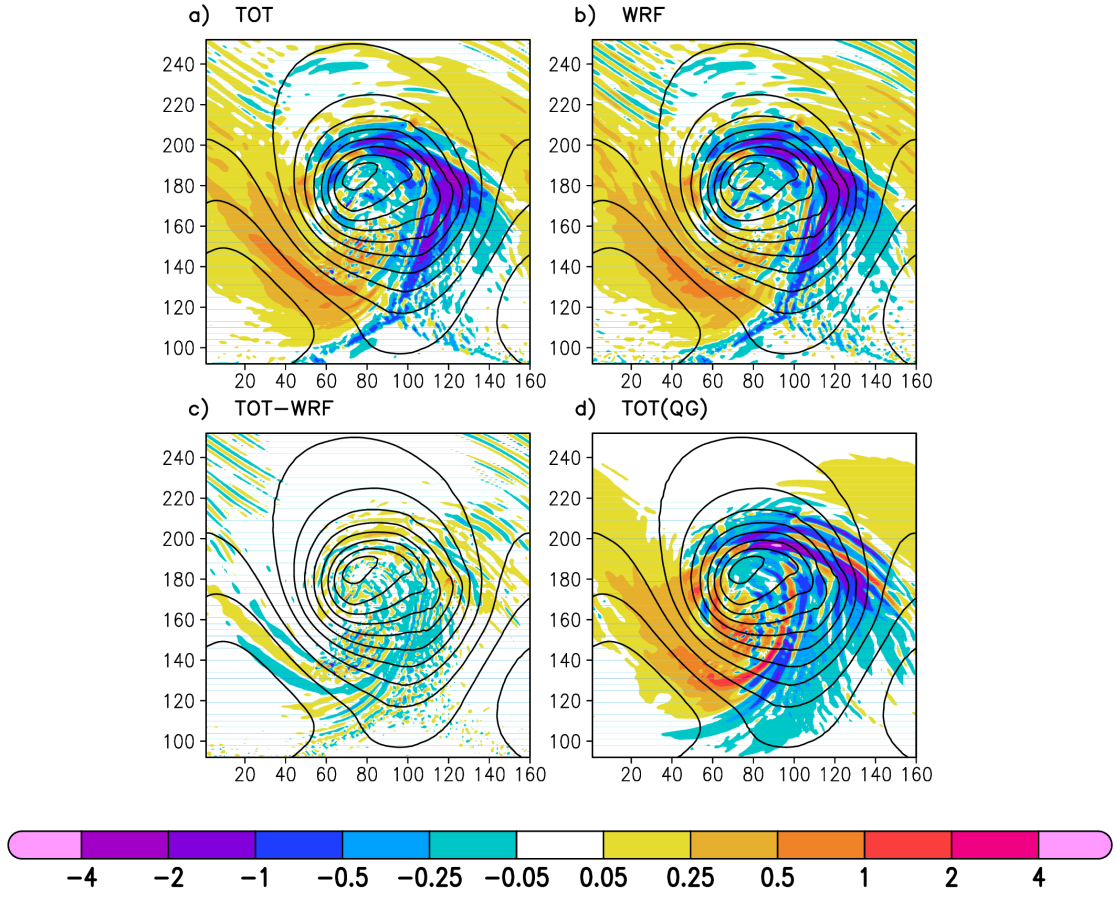

Figure 1: (a) The solution of the generalized omega equation (Eq. 14), (b) the simulated ω directly from the WRF model, (c) their difference, and (d) the solution of the QG omega equation (Eq. 1) at 700 hPa nearly at the time of maximum intensity of the storm simulated in **Paper I**. The contours show the geopotential height at 900 hPa. The labels on the x and y axes indicate grid point numbers. Figure adopted from **Paper I**.

Because the generalized omega equation has been derived directly from the primitive equations, it characterizes atmospheric vertical motion without any simplifying assumptions. Thus, ideally, the correlation against model-resolved vertical motion should be close to 1.0. In fact, this was actually the case in the mid-troposphere, where we documented correlation of 0.95 (**Paper I**) and 0.92 (**Paper III**, blue line in Fig. 2). Near the surface and higher up in the atmosphere the correlation between the generalized omega equation and the model-resolved ω is weaker due to the homogeneous

boundary conditions used in solving the omega equation. Note that in both papers, the correlation was calculated from the area centred at the ETC where the vertical motions are naturally stronger than on average in the atmosphere. When comparing the spatial fields of the solution of generalized omega equation (Fig. 1a) and ω from the WRF model (Fig. 1b), the agreement is excellent. The existing small discrepancies originate from numerical errors, such as the ones arising from the estimation of time derivatives in Eq. 11.

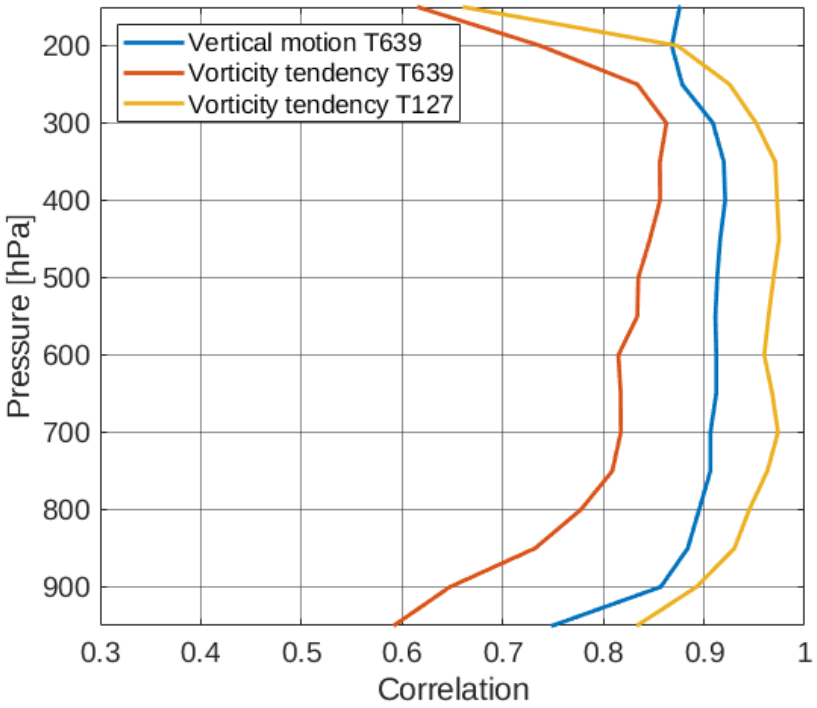

Figure 2: The correlation between the solution of the generalized omega equation and ω from the OpenIFS model (blue), and correlation between the solution of the vorticity equation and the vorticity tendency from OpenIFS at T639 resolution (red) and smoothed to T127 resolution (yellow). The values have been calculated from a 10°x10° moving box centred to the centre of storm Ophelia. Figure adopted from **Paper III**.

2.4.2 Geopotential height tendency and vorticity tendency

As regards the validation of calculated geopotential height tendencies (the sum of the RHS terms in Eq. 20) and vorticity tendencies (the sum RHS terms in Eq. 21), the comparison was made to time derivatives of geopotential height and vorticity fields. The time derivatives were estimated with the central difference method from the actual geopotential height and vorticity fields from the model output. This made the comparison sensitive to the output interval of the model data, since the estimation of the time derivatives improves when the output interval becomes smaller. 30-min output interval was used In **Paper I** and one-hour in **Paper III**, which were compromises between accuracy and the resulting data volume.

For the geopotential height tendency, our diagnostic tool reproduced the time derivative of geopotential height from the model very well, with correlation of 0.95 at 900 hPa and 0.97 at the upper troposphere (not shown) in **Paper I**. Vorticity tendency contains much more small-scale noise than the geopotential height tendency, and thus the correlation is more vulnerable to numerical errors. At T639 resolution, which corresponds to about 30 km grid spacing, the correlation between the solution of the vorticity equation and the time derivative of model-resolved relative vorticity in **Paper III** was 0.65 at 900 hPa, but exceeded 0.85 in the upper troposphere (red line in Fig. 2). When the vorticity tendency fields were smoothed to T127 resolution, the correlation improved to 0.90-0.96 in the free troposphere (yellow line in Fig. 2).

In summary, our diagnostic methods for geopotential height tendency and relative vorticity tendency closed the tendency budgets reasonably well with no considerable residuals. The same was true for the vertical motion calculated with the generalized omega equation (Fig. 1c), but not for the QG omega equation in **Paper I**. Thus, the QG equation was not used further in the meteorological analysis. Our validation results indicate that the equations as well as the numerical methods used in solving them are credible and they can be employed for studying the dynamics of ETCs.

2.5 Cyclone energetics

The cycle of "mechanical energy" in the atmosphere can be depicted with the simple 4-component diagram (Lorenz, 1955) shown in Fig. 3. The two upper boxes describe the storages of available potential energy of the zonal mean flow (A_Z) and the kinetic

energy of the zonal mean flow (K_Z). The lower boxes represent the storages of available potential energy and kinetic energy associated with the atmospheric eddies (A_E and K_E, respectively). The energy of eddies is sometimes decomposed further into the parts associated with stationary and transient eddies (e.g. in Hernández-Deckers and von Storch, 2011), but for simplicity, this division is not made here.

The energy generation terms, the conversion terms between the storages, and the energy dissipation terms have been marked in Fig. 3 with the arrows. The approximate numerical values, according to Boer and Lambert (2008), for both the storages and the conversion terms have also been given.

The main flow of mechanical energy in the atmosphere is marked with the bold arrows in Fig. 3, and can be qualitatively explained as follows:

1) Available potential energy of the zonal mean flow (A_Z), which is the measure of the baroclinicity, is generated (G_Z) continuously when the solar heating tends to increase the meridional temperature differences between low and high latitudes.

2) A_Z is converted into available potential energy of the eddies (A_E) via the conversion term between A_Z and A_E ($C(A_Z, A_E)$), if the meridional heat flux in the eddies is directed towards lower temperatures. This means that the disturbances tend to reduce the meridional temperature differences but increase them in the zonal direction.

3) Within the eddies, if the relatively warm air rises and the cold air sinks, A_E is further converted into kinetic energy of the eddy (K_E). This process is described by the conversion term $C(A_E, K_E)$ in Fig. 3.

4) Finally, most the K_E is destroyed through the dissipation of K_E (D_E). However, about 20 % of the eddy kinetic energy is converted to the kinetic energy of the zonal mean flow via $C(K_E, K_Z)$.

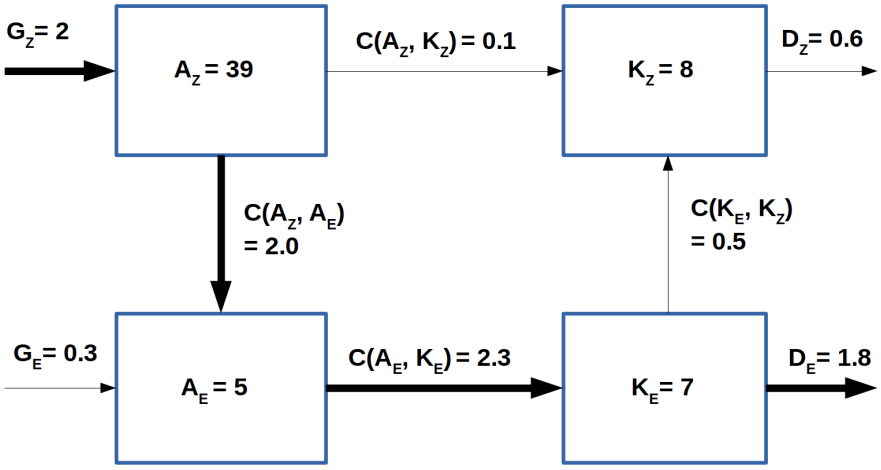

Figure 3: The globally and annually averaged cycle of mechanical energy in the atmosphere. The numerical values are averaged over two reanalysis datasets (Boer and Lambert, 2008). The upper row describes the available potential energy (A_Z) and the kinetic energy (K_Z) of the zonal mean flow, and the lower row describes the available potential energy (A_E) and the kinetic energy (K_E) of the eddies. The unit for storages is 10^5 J/m^2 and for conversions W/m^2. The figure is modified from Fig 4. in Boer and Lambert (2008).

In **Paper II**, the storages A_Z, A_E, and K_E as well as the conversion terms $C(A_Z, A_E)$, $C(A_E, K_E)$ and the dissipation rate D_E were calculated for the model-simulated cyclone in both present-day climate conditions and for three different experiments where the initial temperature distribution was altered. The equations used for the calculation are based on Lorenz (1955) and Oort (1964), and can be found from Section 2.3 of **Paper II**.

3 Physical processes affecting the evolution of extratropical cyclones

The physical processes affecting the evolution of the simulated ETC were studied in **Paper I** and **III**, and partially also in **Paper IV**. In **Paper I**, the contributions of the different physical processes on the life cycle of the ETC were studied using a highly

controlled model configuration where only one ETC was simulated (see Section 2.3.1). In **Paper III**, the main target was to apply the diagnostic method to the extratropical transition of a tropical cyclone, and investigate what is the role of the different processes in an ETC which originates from a strongly diabatically-driven hurricane.

3.1 Idealised simulations

Figure 4 shows the decomposition of atmospheric vertical motion at 700 hPa associated with an idealised ETC in the baroclinic life cycle simulation at the time when the cyclone is close to its maximum intensity. The total vertical motion, which is presented in Fig. 4f, has been obtained by summing the individual terms (Fig. 4a-e) together. The total field is in a very close agreement with the model-resolved vertical motion (as shown earlier in Fig. 1a and b).

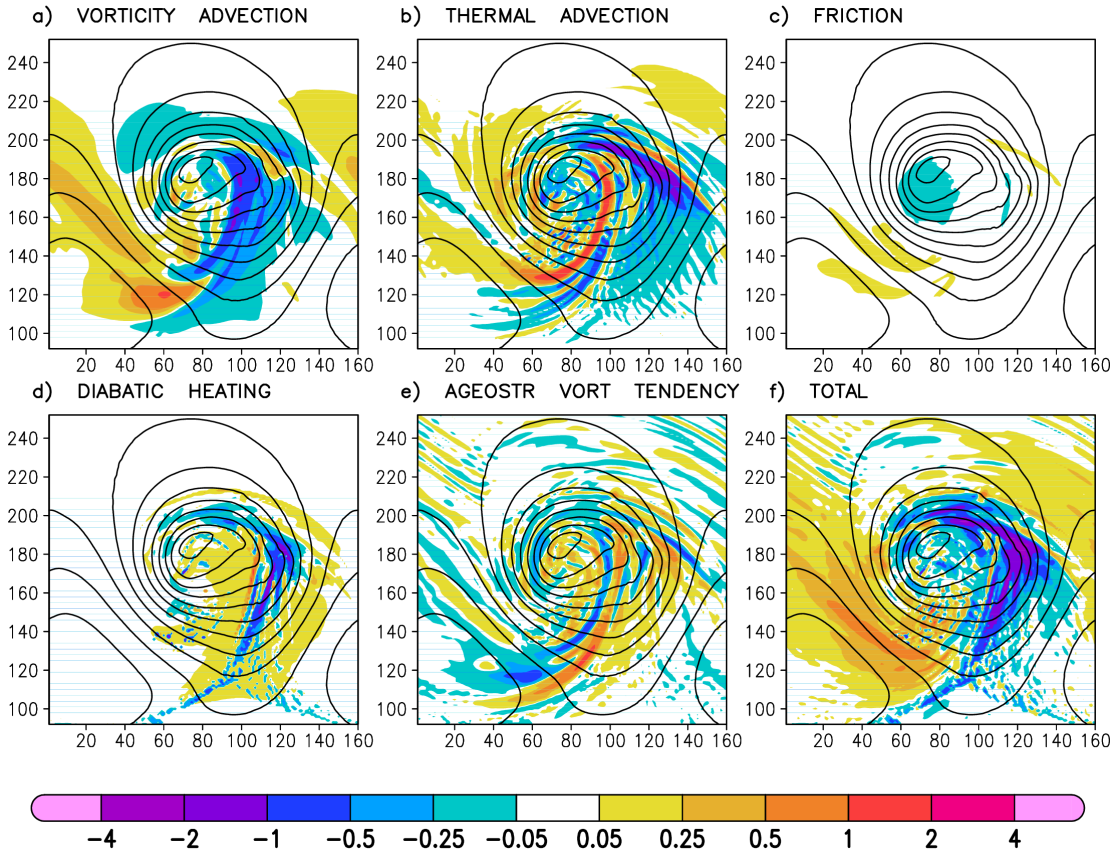

Figure 4: Pressure coordinate vertical motion ω at 700 hPa (colours, with unit of Pa s^{-1}) induced by (a) vorticity advection, (b) thermal advection, (c) friction, (d) diabatic heating, (e) imbalance term, and (f) the total vertical motion. The contours show 900 hPa geopotential height. Figure adopted from **Paper I**.

Omega due to vorticity advection (Fig. 4a) shows large-scale ascent mostly on the southeastern flank of the surface low. In this area, the non-divergent vorticity advection ahead of the upper trough increases upwards which in turn forces ascent in order to maintain hydrostatic balance. The ascent due to thermal advection (Fig. 4b) has more small-scale features, and is maximized in the area of the warm front where the warm air advection is strongest. In the vicinity of the cold front, the effects of vorticity advection and thermal advection seem to compensate each other. This area of cancellation is a well-known feature in ETCs (visible also in Fig. 10 in **Paper IV**) and results from the fact that upward increasing cyclonic vorticity advection and cold-air advection take place in the same area.

Friction causes upward motion near the centre of the low (Fig. 4c) due to the frictional convergence of surface winds and the subsequent Ekman pumping (e.g. Beare, 2007). The magnitude of the ascent is quite weak at 700 hPa, partly due to the fact that the vertical motions induced by friction reach their maximum at lower levels, usually at 900-800 hPa (Stepanyuk et al., 2017). In **Paper III**, we found that the maximum of ascent associated with Ekman pumping rose from 950 hPa to 850 hPa during the extratropical transition of Storm Ophelia.

Diabatic heating, which in the free troposphere in this simulation results from the latent heat release associated with condensation and freezing of water vapor, enhances the rising motion considerably within the frontal zones (Fig. 4d). There are also some small-scale regions of ascent behind the cold front, which are related to the shallow convection taking place when cold air flows above the warm sea surface. Note that latent heat release cannot be considered a totally independent cause of rising motion, but it rather acts as a positive feedback phenomenon which typically requires pre-existing rising motion to occur.

The vertical motion field attributed to the imbalance term (Fig. 4e) is substantial but noisy. One can note the tendency of this term to cancel out the effect of thermal advection (Fig. 4b), especially in the vicinity of the cold front. The reason for this behaviour is that in the atmosphere the temperature tendencies induced by thermal advection are usually small by their temporal and spatial scales, particularly at low levels. However, often the atmosphere does not have time to adjust to these imbalance situations between temperature and vorticity tendencies and thus the compensating vertical motion does not occur. These situations are taken into account by the imbalance term, which often cancels out the effects of thermal advection.

Although these results are directly applicable to the idealised cyclone used in **Paper I**, they reflect the typical distributions of the vertical motions caused by the forcing terms for ETC developed within a baroclinic jet at mid-latitudes over sea surface. In the real world, however, ETCs can be far away from the beautiful, textbook-type cyclones studied in **Paper I**. The variability in the structure and intensity among ETCs stems from the changing contributions of the different forcing mechanisms affecting their evolution. For example, continental cold-season ETCs have often limited access to atmospheric moisture, and thus they are driven more by the dynamical terms (e.g. by vorticity advection in the study by Rolfson and Smith, 1996). On the other hand, ETCs formed above sea surface, and especially those which have tropical origins, are

more diabatically-driven. One example of such a system was Hurricane Ophelia, which underwent an extratropical transition and transformed into a powerful ETC when it hit Europe in October 2017. The contributions of the different physical processes for the low-level cyclone were analysed in **Paper III**, and the main results are presented in the next section.

3.2 Extratropical cyclone transformed from a tropical cyclone

Hurricane Ophelia was a category 3 hurricane which developed over the eastern North Atlantic in October 2017. Ophelia was exceptionally strong for its longitude - National Hurricane Center stated in their post-season report (Stewart, 2018) that Ophelia was the easternmost major hurricane observed in the satellite era. Ophelia underwent an extratropical transition (ET; Sekioka, 1956; Palmén, 1958), a process where the tropical characteristics of the cyclone are replaced by the features typical for ETCs, such as cold core and fronts. The ET of Ophelia was fairly classic; the storm interacted with a positively tilted mid-latitude trough, and the enhanced upper-level divergence due to a favorable position at the right entrance region of the jet stream ensured that Ophelia remained a very strong storm during the ET period. For more detailed synoptic overview of the event, see **Paper III**.

There were two main reasons why we chose a cyclone that transitions from tropical to extratropical as the subject of the case study in **Paper III**. First, we wanted to study a case which would provide a large variety of physical processes affecting to the evolution of the cyclone. Transitioning cyclones are often strongly involved with both thermodynamic and dynamic processes, and thus they can act as good example of such a case. Secondly, to our knowledge, there are no existing literature where the generalized omega equation has been applied to a cyclone with tropical origin.

Figure 5 shows the time series of vorticity tendencies induced by the different forcing terms (RHS terms of Eq. 21) at the cyclone centre. The vorticity tendencies have been averaged over a small circular area following the cyclone centre, which helps to eliminate the vorticity tendency component related to the movement of the storm. Thus, the values in Fig. 5 should represent the changes in the cyclone's intensity. A positive vorticity tendency means that the low-level vorticity at the storm's centre is increasing, which in turn reflects an increased intensity of the cyclone. The approximate times of tropical, transition, and extratropical phases of Ophelia were determined using

a cyclone phase space diagram (Hart, 2003; Evans and Hart, 2003) and the post-season report by the National Hurricane Center (Stewart, 2018).

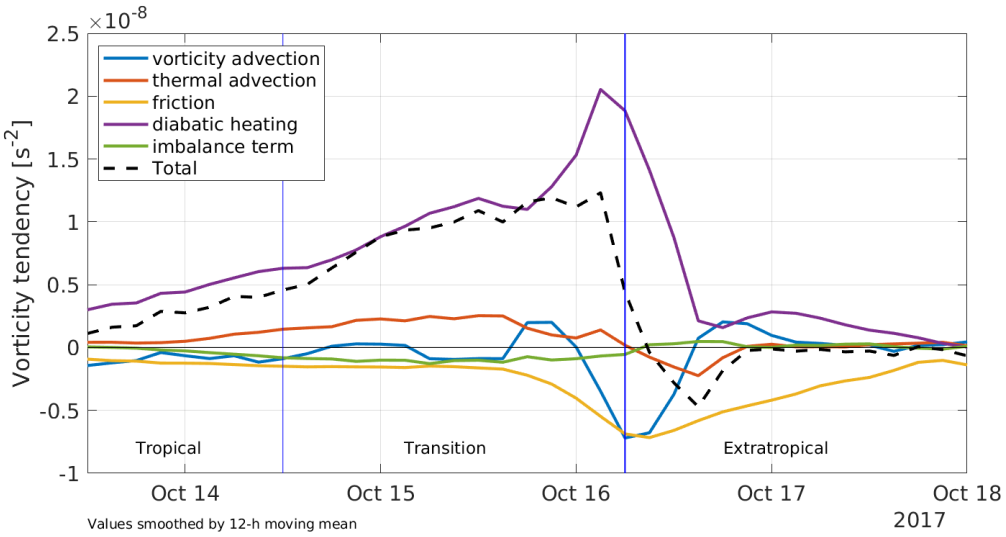

Figure 5: The time evolution of vorticity tendencies due to different forcing terms. The values have been averaged over the 900–800-hPa layer and over a circular area with a 1.5° radius centred on the maximum of the T127 vorticity field. In addition, the values are 12-hour moving averages. The vertical lines mark the approximate times of tropical, transition, and extratropical phases of the storm. Figure is modified from **Paper III**.

The striking feature in Fig. 5 is the dominance of diabatic heating (purple line) during the tropical, transition and extratropical phases of the storm. Furthermore, the contribution of diabatic heating increased during the life cycle, and peaked just when Ophelia was reaching its extratropical phase. In **Paper III**, we found that most of the low-level vorticity tendency at the centre of the cyclone in the tropical phase was generated via the convection scheme of the model. In contrast, the microphysics scheme was responsible for most of the low-level vorticity tendency at the cyclone's centre in the extratropical phase. This shift from convection scheme to microphysics scheme illustrates how the near-core convection transformed into large-scale ascent during the ET of Ophelia. Furthermore, it would be interesting to perform a more comprehensive analysis of whether this feature could be used as a proxy in objectively identifying the tropical, transition and extratropical phases of the transitioning storms.

Another interesting finding was the neutral, or even negative contribution from the vorticity advection (blue line in Fig. 5) to the evolution of the low-level vortex. In the tropical phase and during most of the transition period, the vorticity tendency by vorticity advection at the cyclone centre was close to zero. However, when the cyclone reached its extratropical phase, the low-level vorticity tendency that was due to vorticity advection became markedly negative, to the level of magnitude attributed to the friction term. We found that this behaviour was due to the secondary circulation of the cyclone. The low-level convergent winds transported air with lower cyclonic vorticity to the centre of the storm, and, thus, reduced effectively the vorticity maximum associated with the storm's centre. Similar results have been found earlier for example by DiMego and Bosart (1982) and Räisänen (1997). In **Paper III**, we speculate that the importance of non-divergent vorticity advection is probably larger higher up in the atmosphere in triggering the vertical motion required for the formation of latent heat release above the low-level vortex. This hypothesis is supported by the favourable interaction of Ophelia with the upper-level trough, as explained in more detail in **Paper III**.

Thermal advection was contributing positively particularly during the transition period (red line in Fig. 5), when warm, subtropical airmass was pushed towards mid-latitudes along with Ophelia. The situation changed during the extratropical phase, when the storm occluded and polar maritime airmass wrapped around the cyclone's warm core. The overall contribution from thermal advection is however quite weak, as the advection term right at the low-level centre must be zero by definition.

To conclude the results from **Paper III**, it can be stated that baroclinic processes played a relatively small role for the generation of low-level vorticity during the post-ET intensification period of Ophelia. Instead, we find that diabatic heating, dominated by the convection in the tropical phase and the large-scale ascent in the extratropical phase, was the leading forcing in the strengthening of Ophelia. However, it should be kept in mind that we analysed the vorticity tendencies only for the surface cyclone, and thus the results are not applicable at higher levels, where the baroclinic forcings were presumably more important. Based on only one case study, it is difficult to say whether our results are typical for transitioning tropical cyclones. In **Paper I** we performed similar analysis for a regular, idealized ETC, and found that adiabatic processes played approximately an equally important role as diabatic processes.

4 Effect of warmer climate

This section focuses on how the structure and energy cycle of ETCs will change with climate change. In the first subsection, the changes in the structure of the cyclones with the warming are discussed. The changes in the structure of ETCs were investigated partly in **Paper II** with WRF model, but more comprehensively in **Paper IV** with OpenIFS model. These structural changes in the cyclones with the warming lead to changes also in their energy cycle, which was investigated in **Paper II**.

4.1 Changes in the characteristics and structure of the cyclones

In **Paper II** and **IV**, and in line with the existing literature, we found that ETCs which form in a warmer environment have some characteristics that are different from those that form in a colder environment. The main reason for the differences is the increased atmospheric moisture content, as the warmer air can naturally hold more moisture. In short, the higher moisture content means that diabatic processes in the cyclone become more prevalent during its evolution.

In **Paper II**, the cyclone which developed in 6 K warmer environment deepened more rapidly and ended up being about 7 hPa deeper than the cyclone in the control simulation. The faster deepening was linked to the enhanced release of latent heat above the surface low. Moreover, the heating above the low and the subsequent deepening did not occur steadily, but there were clearly identifiable deepening periods during the life cycle of the storm. In contrast, the cyclone in the present-day environment deepened more gradually, owing this behaviour to more dynamic influences rather than diabatic processes. The faster deepening rate in ETCs formed in warmer and moister conditions is also supported by the findings of **Paper IV**: the strongest 200 cyclones in the warmer climate deepened approximately 25 % faster than the strongest 200 in the present climate. However, when all ETCs were considered (instead of the strongest 200), on average there was no change in the deepening rate.

When looking at the structural changes of ETCs with the warming, a common result from the numerical simulations in **Paper II** and **IV** was the expansion of the area of ascent to downstream of the cyclone centre. This feature is well seen in Figure

6, which shows the 700-hPa vertical motion and its response for the warming in the composite ETC 24 hours before the time of maximum intensity (Fig. 6a) and at the time of maximum intensity (Fig. 6b). The ascent at both panels is maximised to the eastern side of the low (similarly as in Fig. 4f), in the warm sector region where the warm conveyor belt of the low is situated. However, in the experiment where the SSTs were warmed by 4 K, the ascent does not increase precisely at its maximum area, but rather on the poleward and downstream side of the present-day maximum. This result is in line with **Paper II**, where we found that the area of warm-frontal ascent migrated eastward and coincided less well with the warm sector when the atmospheric temperature was increased (see Fig. 6 in **Paper II**).

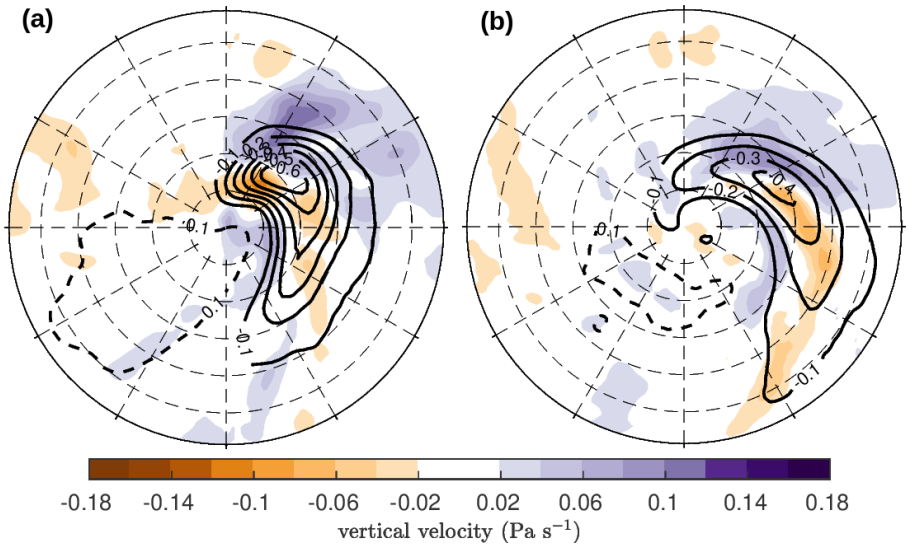

Figure 6: Composite mean and change in 700-hPa vertical velocity in pressure coordinates at (a) 24 hours before the time of maximum intensity and (b) at the time of maximum intensity. Contours show the control values and shading the difference with the warming. Both panels are the composites of the strongest 200 ETCs in each experiment. Modified from **Paper IV**.

A natural follow-up question is then which processes cause the expansion of ascent downstream of the cyclone centre. We discovered that the cyclone-related ascent changes in a complex manner. Firstly, the ascent attributed to thermal advection shifts more poleward relative to the cyclone centre (Fig. 7a). We conclude that this is related to movement of the warm front further away from the cyclone centre with the warming, resulting in a decrease of ascent (or increase of descent) near the cy-

clone centre. However, the primary reason for the downstream increase of ascent is the broadening of the upper-level trough, which induces more upward motion via forcing of vorticity advection (Fig. 7b). Finally, due to increased moisture content, the release of latent heat and thus ω attributed to diabatic heating will strengthen. This is projected to occur mainly within the warm front where the precipitation is strongest. In summary, all these three processes contribute to the increase of ascent downstream and poleward relative to the center of the composite cyclone, but the most pronounced and geographically widest response seems to originate from the vorticity advection term.

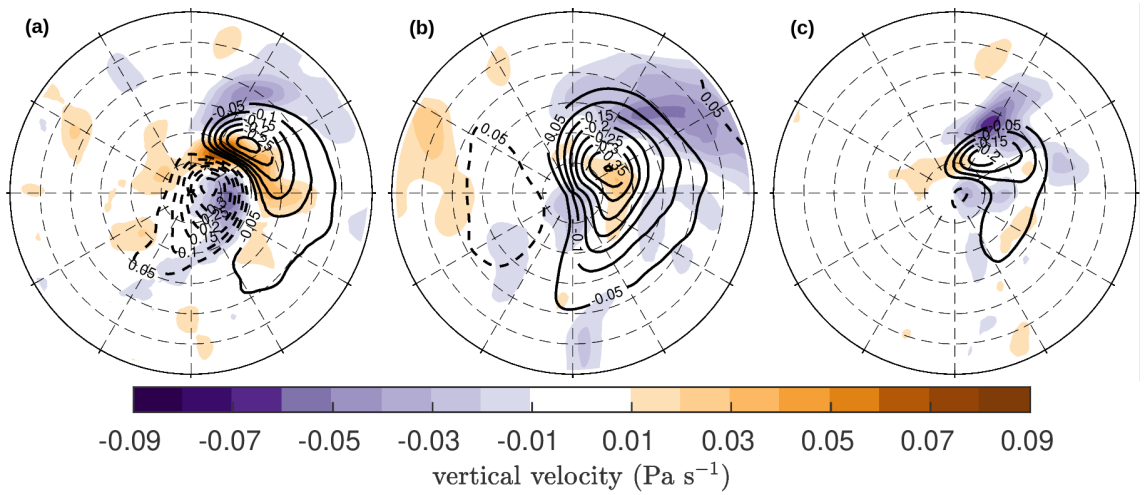

Figure 7: Composite mean and change in 700-hPa vertical velocity in pressure coordinates due to a) thermal advection, b) vorticity advection and c) diabatic heating at 24 hours before the time of maximum intensity. Contours show the control values and shading the difference with the warming. All composites are of the strongest 200 extra-tropical cyclones in each experiment.Modified from **Paper IV**.

While the area of ascent caused by vorticity advection moves slightly downstream due to the broader upper-level trough, the absolute maximum of ascent attributed to vorticity advection decreases slightly. Furthermore, a small decrease in the maximum values of ascent due to thermal advection was also found to take place with the warming. In contrast, the maximum of ascent attributed to diabatic heating increased slightly. Thus, the upward motion in ETCs is expected to become more diabatically-driven in the warmer climate. The numerical values for the maximum values are given in Table 2 of **Paper IV**.

We also found in **Paper IV** that vertical motions in ETCs became slightly more

asymmetric with the warming (not shown). Specifically, the increased asymmetry stems from the fact that the mean upward motion averaged over the composite cyclone area was found to grow in absolute terms, while the mean downward motion was found to weaken. No changes in the fractional area of ascent in ETCs were observed.

As a natural consequence of the fact that there is more moisture in the warmer climate, the precipitation associated with ETCs will increase. According to the simulations performed in **Paper IV**, the cyclone-related total precipitation increased by up to 50 % with the 4-K warming. Furthermore, the response of total precipitation was partitioned into contributions from large-scale precipitation and convective precipitation. It was found out that the maximum of large-scale precipitation moves spatially poleward with the warming, while the area of convective precipitation remains approximately at the same area. The poleward shift in large-scale precipitation is in line with the changes in the area of large-scale ascent presented earlier.

Finally, the 900–700-hPa potential vorticity (PV) was found to increase at all stages of the cyclone evolution. The largest increase of PV is expected to occur slightly poleward from the cyclone centre, which results from the expansion of ascent and the consequent enhanced large-scale precipitation. This induces diabatically more low-level PV in that region via enhanced latent heating. Elsewhere in the surroundings of the storm centre, a small increase of PV was found to take place due to increased stratification.

4.2 Changes in the energy cycle of cyclones

As seen from Fig. 3, the main energy cycle of the atmosphere is dependent on the existence of eddies. These eddies, which consist largely of ETCs, are a crucial part of the atmospheric general circulation. In a warmer climate, the structure of ETCs, and hence their ability to convert atmospheric potential energy into kinetic energy could be changed, which has effects eventually for the whole general circulation. In **Paper II**, the energy cycle of the WRF-simulated ETC was investigated using three different climate change scenarios which were incorporated to the initial state of the model one at a time (see Section 2.3.1).

The main outcome in the simulations conducted in the warmer environment was that the increased atmospheric temperature and hence the moisture content compared to typical present-day values decreased the capability of the cyclone to exploit the avail-

able potential energy of the zonal mean flow (A_Z). This can be seen from Fig. 8a as a smaller decrease of A_Z with time in the warmer simulation (red solid line) compared to the control simulation (blue solid line), and from Fig. 8d as a weaker conversion of A_Z to available potential energy of the eddy (A_E).

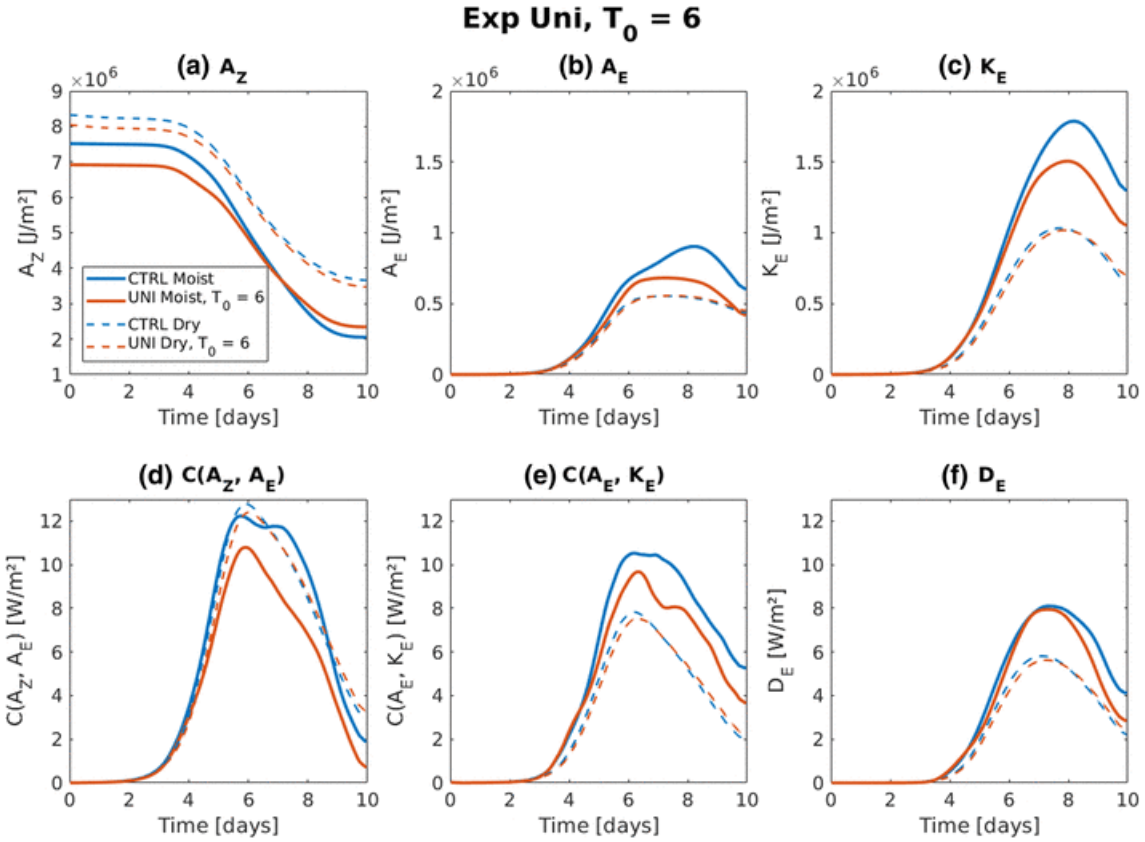

Figure 8: Time evolution of (a) available potential energy of the zonal mean flow (A_Z), (b) available potential energy of the eddy (A_E), (c) kinetic energy of the eddy (K_E), (d) energy conversion from A_Z to A_E, (e) energy conversion from A_E to K_E, and (f) the dissipation rate of K_E. The dashed lines indicate simulations without atmospheric moisture and solid lines with moist environment. The blue lines (both dashed and solid) depict the control runs and the red lines depict the runs where temperature has been increased uniformly by 6 K. Figure adopted from **Paper II**.

Due to the weaker conversion from A_Z to A_E, the maximum of A_E remained about 25% smaller in the warmer environment (red solid line in Fig. 8b) than in the control run (blue solid line). The reason for this behaviour remained slightly unclear, but we suspect that the weakening of the jet stream by 1.5 m s^{-1} with the warming may play a

role, via weaker meridional heat flux which acts to generate A_E in the atmosphere. The weaker jet stream results from the uniform warming: with fixed surface pressure, the geopotential heights increased more in the northern part of the domain where the initial temperature was lower, which then acted to reduce the meridional pressure gradient and caused the deceleration of the initial zonal wind speed.

As expressed earlier, the cyclones in warmer environment are expected to intensify more rapidly and their minimum surface pressure may be lower due to increased diabatic processes. However, despite the fact that they may be deeper, the kinetic energy of these systems (K_E) may be actually lower, as seen from Fig. 8c. We suspect that this behaviour is related to the fact that the pressure minimum caused by diabatic processes can be very localised and small-scale, which does not affect considerably K_E averaged over the whole model domain, and moreover, the major contribution to K_E comes from the upper troposphere where the winds are strongest.

The physical reason for about 15 % lower K_E with the warming originates presumably from the structural changes of the ETC. We found that the core of the rising motion shifted downstream with the warming - a result which was found earlier in other studies (e.g. in Kirshbaum et al., 2018), and was confirmed later in **Paper IV**. Due to the downstream migration of ascent, the warm sector coincided less well with the area of rising motion in the eddy. Since K_E is produced when relatively warm air rises, the worse phasing between temperature and vertical motion decreases effectively the production of K_E. This reduced production of K_E in the warmer environment (red solid line) than in the control simulation (blue solid line) is seen in Fig. 8e.

In **Paper II**, we also performed two additional numerical experiments where we modified the meridional temperature gradient of the environment. Firstly, the main outcome from the experiment with reduced low-level temperature gradient was that the resulting cyclone was weaker in terms of maximum of A_E and K_E in both dry and moist simulations (not shown, see **Paper II**). This highlights the fact the low-level temperature gradient has a substantial control over the ETC intensity which results from the decreased baroclinic processes rather than the diabatics.

Secondly, we discovered that the energy cycle of the idealized ETC responds differently to the changes in the lower and upper level temperature gradient. While modifying the lower level temperature gradient had a clear effect on A_E and K_E in both dry and moist simulations, modifying the upper-level temperature gradient provided slightly weaker

control (not shown, see **Paper II**). Furthermore, the response to increased upper level temperature gradient was different depending on the presence of atmospheric moisture. In the dry environment, the interaction between upper and lower level waves was weaker, and thus the increase of baroclinicity at upper levels was not materialized as higher K_E. In the moist atmosphere, in contrast, the mid-tropospheric latent heating acted as a link between the upper and lower PV anomalies and thus the increased baroclinicity in the upper troposphere was reflected more efficiently in the intensity of the simulated cyclone, increasing thus also K_E.

As a summary of **Paper II**, it can be said that both the uniform warming of the atmosphere and the decrease of the lower-level temperature gradient tend to reduce the energy of ETCs. Because both phenomena are taking place simultaneously in the northern mid-latitudes, it is expected that in the future climate, the kinetic energy associated with ETCs will potentially decrease. However, more research is needed to make further conclusions, especially because in our simulations the temperature changes were conducted one at a time while in the real world they are occurring simultaneously. Given the possible nonlinear responses and also the increase of the upper-level temperature gradient, drawing direct conclusions to the real world must be done with caution.

5 Discussion and conclusions

This thesis contributed to understanding of (1) the role of various synoptic-scale forcing terms to the evolution of ETCs and (2) the effects of warmer climate to the characteristics and structure of ETCs. The point (1) was studied with the diagnostic tools which consisted of the generalized omega equation and either the Zwack-Okossi equation or the traditional vorticity equation. The diagnostic tools were applied to an idealised, text-book type of ETC as well as a real-world, post-tropical ETC. These two cases represented very different examples of ETCs in terms of their synoptic evolution and the used model configuration.

The diagnostic tools performed well in reproducing the total atmospheric vertical motion, geopotential height tendency, and vorticity tendency when those quantities were compared to the corresponding model-simulated fields. The applied decomposition revealed the contributions of different physical processes behind the total fields. While both adiabatic and diabatic processes were important for the development of the idealized ETC, the transitioned ex-hurricane was strongly driven by diabatic processes.

The diagnostic method presented in this thesis has the advantage that vertical motion is partitioned into its causes rather than treated as an independent forcing for weather systems. In many earlier diagnostic studies (e.g. Azad and Sorteberg, 2009; Fu et al., 2018) the adiabatic heating/cooling associated with vertical motions is interpreted as an independent forcing, which is problematic due to the strong tendency of vertical motions to compensate the effect of other physical processes.

Our finding that the simulated cyclone in the warmer environment in **Paper II** was unable to exploit the atmospheric baroclinicity as efficiently as the cyclone in the control simulation was consistent with Tierney et al. (2018) but contrary to Kirshbaum et al. (2018). However, the results obtained from baroclinic wave simulations can be surprisingly sensitive to the initial jet stream configuration, as shown in Kirshbaum et al. (2018). Furthermore, Kirshbaum et al. (2018) also stress the fact that the simulated ETC may start to unphysically interact with itself in the channel mode simulations, which is naturally not a desirable feature. Nevertheless, the decreased conversion from A_E to K_E and, thus, eventually the lower K_E with the uniform warming reported in **Paper II** seems to be a more robust result, which is confirmed by numerous other studies with idealized baroclinic waves (e.g. Booth et al., 2013; Tierney et al., 2018; Kirshbaum et al., 2018) and also with global model simulations (e.g. O'Gorman, 2011;

Pfahl et al., 2015).

The results from the simulations conducted in the warmer climate in **Paper IV** suggest faster deepening rate and larger number of extreme ETCs, in line with Büeler and Pfahl (2019), who also reported that the most intense ETCs could reach higher intensity in warmer climates. However, these results seem to be inconsistent with simulations performed with fully coupled climate models (Bengtsson et al., 2009; Catto et al., 2011; Seiler and Zwiers, 2016). This may be due to the absence of Arctic amplification in our model set-ups, which decreases the lower level meridional temperature gradient and reduces the ETC intensity, as evidenced in **Paper II**. Thus, the results expressed in **Paper IV** may be more applicable to the southern hemisphere in this sense, but they also confirm the impact of Arctic amplification on the intensity of ETCs.

While it is evident that simulating one ETC with baroclinic wave configurations has its limitations when attempting to draw conclusions to real-world changes in ETCs, the aqua-planet configuration used in **Paper IV** serves a useful intermediate step which accounts for example the non-linear interactions between the eddies. However, one interesting step forward from **Paper IV** would be to add the polar amplification to the simulations and see how the intensity and structure of ETCs respond to both warming and the decrease of lower level temperature gradient simultaneously, similarly as in the real world.

In the future, it would be valuable to develop further the diagnostic software to be easier to adopt by different end-users. This would need additional programming to make the tool fit seamlessly for different model outputs, and run with different super-computer environments. As regards scientific future directions, it would be interesting to conduct more comprehensive analysis on the forcing term contributions for ETC development and investigate for example their geographical or seasonal differences, or target the study only to transitioning cyclones and explore whether our findings in the Ophelia case can be generalized for other cyclones undergoing extratropical transition. The tool could also be applied to climate change simulations with OpenIFS, and investigate how much the contributions of different adiabatic and diabatic terms to the intensity of ETCs change with the warming.

6 Review of papers and the author's contribution

This thesis consists of four peer-reviewed publications that aim to increase the general knowledge on the dynamics of ETCs by (1) presenting and applying the diagnostic method for an idealized baroclinic wave (**Paper I**) and a real-world case study (**Paper III**), and (2) studying how ETCs respond to climate change in idealized baroclinic wave simulations (**Paper II**) and global model simulations with intermediate complexity (**Paper IV**).

Paper I acts as a documentation of the diagnostic method which can be used for idealized baroclinic wave simulations by the Weather Research and Forecasting (WRF) model or similar models which employ Cartesian coordinate system. The author contributed to the software development, did the meteorological analysis and wrote most of the manuscript.

Paper II provides insight into how sensitive the different energy quantities and the conversions between them are for the anticipated temperature changes in the future climate. We also made an attempt to identify which structural changes of ETCs are behind the changes of energetics. The author performed the model simulations, analysed the results together with the co-authors, and was responsible of writing the paper.

Paper III extends the method used in **Paper I** for global model output on a spherical grid rather than Cartesian. We demonstrate the method by analysing the synoptic-scale forcing terms affecting the extratropical transition of Hurricane Ophelia (2017). The author contributed to the technical development of the diagnostic method. The application of the tool, most of the analysis, and almost all of the writing were performed by the author.

Paper IV investigates the changes in the characteristics and structure of ETCs with the warming of climate by using 10 year-long aqua-planet simulations. The paper extends the topic of **Paper II** into a global domain and beyond one cyclone to much larger sample size. The author performed the decomposition of the vertical motion with the diagnostic omega equation tool, and contributed to analysing and discussing the results, together with the first author and the other co-authors.

References

Ahmadi-Givi, F., Graig, G., and Plant, R. (2004). The dynamics of a midlatitude cyclone with very strong latent-heat release. *Quarterly Journal of the Royal Meteorological Society*, 130(596):295–323.

Allen, R. J. and Sherwood, S. C. (2008). Warming maximum in the tropical upper troposphere deduced from thermal winds. *Nature Geoscience*, 1(6):399.

Azad, R. and Sorteberg, A. (2009). A diagnosis of warm-core and cold-core extratropical cyclone development using the Zwack–Okossi equation. *Atmospheric Science Letters*, 10(4):220–225.

Azad, R. and Sorteberg, A. (2014a). The vorticity budgets of North Atlantic winter extratropical cyclone life cycles in MERRA reanalysis. Part I: development phase. *Journal of the Atmospheric Sciences*, 71(9):3109–3128.

Azad, R. and Sorteberg, A. (2014b). The vorticity budgets of North Atlantic winter extratropical cyclone life cycles in MERRA reanalysis. Part II: decaying phase. *Journal of the Atmospheric Sciences*, 71(9):3129–3143.

Beare, R. J. (2007). Boundary layer mechanisms in extratropical cyclones. *Quarterly Journal of the Royal Meteorological Society*, 133(623):503–515.

Bengtsson, L., Hodges, K. I., and Keenlyside, N. (2009). Will extratropical storms intensify in a warmer climate? *Journal of Climate*, 22(9):2276–2301.

Boer, G. and Lambert, S. (2008). The energy cycle in atmospheric models. *Climate Dynamics*, 30(4):371–390.

Booth, J. F., Wang, S., and Polvani, L. (2013). Midlatitude storms in a moister world: lessons from idealized baroclinic life cycle experiments. *Climate Dynamics*, 41(3-4):787–802.

Büeler, D. and Pfahl, S. (2017). Potential vorticity diagnostics to quantify effects of latent heating in extratropical cyclones. Part I: methodology. *Journal of the Atmospheric Sciences*, 74(11):3567–3590.

Büeler, D. and Pfahl, S. (2019). Potential vorticity diagnostics to quantify effects of latent heating in extratropical cyclones. Part II: application to idealized climate change simulations. *Journal of the Atmospheric Sciences*, 76(7):1885–1902.

Caron, J.-F., Zwack, P., and Pagé, C. (2006). Dionysos: A diagnostic tool for numerically-simulated weather systems. *Technical related document see http://www.dionysos.uqam.ca/doc/Dionysos.pdf*.

Catto, J. L., Ackerley, D., Booth, J. F., Champion, A. J., Colle, B. A., Pfahl, S., Pinto, J. G., Quinting, J. F., and Seiler, C. (2019). The future of midlatitude cyclones. *Current Climate Change Reports*.

Catto, J. L., Shaffrey, L. C., and Hodges, K. I. (2010). Can climate models capture the structure of extratropical cyclones? *Journal of Climate*, 23(7):1621–1635.

Catto, J. L., Shaffrey, L. C., and Hodges, K. I. (2011). Northern hemisphere extratropical cyclones in a warming climate in the HiGEM high-resolution climate model. *Journal of Climate*, 24(20):5336–5352.

Chagnon, J., Gray, S., and Methven, J. (2013). Diabatic processes modifying potential vorticity in a North Atlantic cyclone. *Quarterly Journal of the Royal Meteorological Society*, 139(674):1270–1282.

Chang, E. K. (2018). CMIP5 projected change in Northern Hemisphere winter cyclones with associated extreme winds. *Journal of Climate*, 31(16):6527–6542.

Chang, E. K., Guo, Y., and Xia, X. (2012). CMIP5 multimodel ensemble projection of storm track change under global warming. *Journal of Geophysical Research: Atmospheres*, 117(D23).

Charney, J. G. (1947). The dynamics of long waves in a baroclinic westerly current. *Journal of Meteorology*, 4(5):136–162.

Collins, M., Knutti, R., Arblaster, J., Dufresne, J.-L., Fichefet, T., Friedlingstein, P., Gao, X., Gutowski, W. J., Johns, T., Krinner, G., et al. (2013). Long-term climate change: projections, commitments and irreversibility. In *Climate Change 2013: The Physical Science Basis. Contribution of Working Group I to the Fifth Assessment Report of the Intergovernmental Panel on Climate Change*, pages 1029–1136. Cambridge University Press.

Dacre, H., Hawcroft, M., Stringer, M., and Hodges, K. (2012). An extratropical cyclone atlas: a tool for illustrating cyclone structure and evolution characteristics. *Bulletin of the American Meteorological Society*, 93(10):1497–1502.

Dacre, H. F., Martinez-Alvarado, O., and Mbengue, C. O. (2019). Linking atmospheric rivers and warm conveyor belt airflows. *Journal of Hydrometeorology*, 20(6):1183–1196.

Davis, C. A. and Emanuel, K. A. (1991). Potential vorticity diagnostics of cyclogenesis. *Monthly Weather Review*, 119(8):1929–1953.

DiMego, G. J. and Bosart, L. F. (1982). The transformation of Tropical Storm Agnes into an extratropical cyclone. Part II: moisture, vorticity and kinetic energy budgets. *Monthly Weather Review*, 110(5):412–433.

Eady, E. T. (1949). Long waves and cyclone waves. *Tellus*, 1(3):33–52.

ECMWF (2014). Documentation–Cy40r1 Part IV: Physical processes. *European Centre for Medium-Range Weather Forecasts: Reading, UK*.

Ertel, H. (1942). Ein neuer hydrodynamischer wirbelsatz. *Meteorologische Zeitschrift*, 59:277–281.

Evans, J. L. and Hart, R. E. (2003). Objective indicators of the life cycle evolution of extratropical transition for Atlantic tropical cyclones. *Monthly Weather Review*, 131(5):909–925.

Fink, A. H., Pohle, S., Pinto, J. G., and Knippertz, P. (2012). Diagnosing the influence of diabatic processes on the explosive deepening of extratropical cyclones. *Geophysical Research Letters*, 39(7).

Fu, S.-M., Sun, J.-H., Li, W.-L., and Zhang, Y.-C. (2018). Investigating the mechanisms associated with the evolutions of twin extratropical cyclones over the northwest Pacific Ocean in mid-January 2011. *Journal of Geophysical Research: Atmospheres*, 123(8):4088–4109.

Grams, C. M. and Archambault, H. M. (2016). The key role of diabatic outflow in amplifying the midlatitude flow: A representative case study of weather systems surrounding western North Pacific extratropical transition. *Monthly Weather Review*, 144(10):3847–3869.

Grams, C. M. and Blumer, S. R. (2015). European high-impact weather caused by the downstream response to the extratropical transition of North Atlantic Hurricane Katia (2011). *Geophysical Research Letters*, 42(20):8738–8748.

Hart, R. E. (2003). A cyclone phase space derived from thermal wind and thermal asymmetry. *Monthly weather review*, 131(4):585–616.

Hartmann, D. L. (2015). *Global physical climatology*, volume 103. Newnes.

Hartmann, D. L., Tank, A. M. K., Rusticucci, M., Alexander, L. V., Brönnimann, S., Charabi, Y. A. R., Dentener, F. J., Dlugokencky, E. J., Easterling, D. R., Kaplan, A., et al. (2013). Observations: Atmosphere and Surface. In *Climate Change 2013: The Physical Science Basis. Contribution of Working Group I to the Fifth Assessment Report of the Intergovernmental Panel on Climate Change*, pages 159–254. Cambridge University Press.

Hawcroft, M., Walsh, E., Hodges, K., and Zappa, G. (2018). Significantly increased extreme precipitation expected in Europe and North America from extratropical cyclones. *Environmental Research Letters*, 13(12):124006.

Hernández-Deckers, D. and von Storch, J.-S. (2011). The energetics response to a warmer climate: relative contributions from the transient and stationary eddies. *Earth System Dynamics*, 2:105–120.

Hodges, K. (1995). Feature tracking on the unit sphere. *Monthly Weather Review*, 123(12):3458–3465.

Hodges, K. I. (1994). A general method for tracking analysis and its application to meteorological data. *Monthly Weather Review*, 122(11):2573–2586.

Hoskins, B. J., McIntyre, M. E., and Robertson, A. W. (1985). On the use and significance of isentropic potential vorticity maps. *Quarterly Journal of the Royal Meteorological Society*, 111(470):877–946.

Kirshbaum, D., Merlis, T., Gyakum, J., and McTaggart-Cowan, R. (2018). Sensitivity of idealized moist baroclinic waves to environmental temperature and moisture content. *Journal of the Atmospheric Sciences*, 75(1):337–360.

Knippertz, P. and Fink, A. H. (2008). Dry-season precipitation in tropical West Africa and its relation to forcing from the extratropics. *Monthly Weather Review*, 136(9):3579–3596.

Knippertz, P., Fink, A. H., and Pohle, S. (2009). Comments on "Dry-season precipitation in tropical West Africa and its relation to forcing from the extratropics" reply. *Monthly Weather Review*, 137(9):3151–3157.

Kuo, Y.-H., Shapiro, M., and Donall, E. G. (1991). The interaction between baroclinic and diabatic processes in a numerical simulation of a rapidly intensifying extratropical marine cyclone. *Monthly Weather Review*, 119(2):368–384.

Kuwano-Yoshida, A. and Enomoto, T. (2013). Predictability of explosive cyclogenesis over the northwestern Pacific region using ensemble reanalysis. *Monthly Weather Review*, 141(11):3769–3785.

Lavers, D. A., Allan, R. P., Wood, E. F., Villarini, G., Brayshaw, D. J., and Wade, A. J. (2011). Winter floods in Britain are connected to atmospheric rivers. *Geophysical Research Letters*, 38(23).

Lee, S. H., Williams, P. D., and Frame, T. H. (2019). Increased shear in the North Atlantic upper-level jet stream over the past four decades. *Nature*, 572(7771):639–642.

Liberato, M., Pinto, J., Trigo, R., Ludwig, P., Ordóñez, P., Yuen, D., and Trigo, I. (2013). Explosive development of winter storm Xynthia over the subtropical North Atlantic ocean. *Natural Hazards and Earth System Sciences*, 13(9):2239–2251.

Liberato, M. L., Pinto, J. G., Trigo, I. F., and Trigo, R. M. (2011). Klaus–an exceptional winter storm over northern Iberia and southern France. *Weather*, 66(12):330–334.

Lorenz, E. N. (1955). Available potential energy and the maintenance of the general circulation. *Tellus*, 7(2):157–167.

Lupo, A. R. and Smith, P. J. (1998). The interactions between a midlatitude blocking anticyclone and synoptic-scale cyclones that occurred during the summer season. *Monthly Weather Review*, 126(2):502–515.

Lupo, A. R., Smith, P. J., and Zwack, P. (1992). A diagnosis of the explosive development of two extratropical cyclones. *Monthly Weather Review*, 120(8):1490–1523.

Martínez-Alvarado, O., Gray, S. L., and Methven, J. (2016). Diabatic processes and the evolution of two contrasting summer extratropical cyclones. *Monthly Weather Review*, 144(9):3251–3276.

O'Gorman, P. A. (2011). The effective static stability experienced by eddies in a moist atmosphere. *Journal of the Atmospheric Sciences*, 68(1):75–90.

O'Gorman, P. A. and Schneider, T. (2008). Energy of midlatitude transient eddies in idealized simulations of changed climates. *Journal of Climate*, 21(22):5797–5806.

Oort, A. H. (1964). On estimates of the atmospheric energy cycle. *Monthly Weather Review*, 92.

Pagé, C., Fillion, L., and Zwack, P. (2007). Diagnosing summertime mesoscale vertical motion: Implications for atmospheric data assimilation. *Monthly Weather Review*, 135(6):2076–2094.

Palmén, E. (1958). Vertical circulation and release of kinetic energy during the development of Hurricane Hazel into an extratropical storm. *Tellus*, 10(1):1–23.

Pauley, P. M. and Nieman, S. J. (1992). A comparison of quasigeostrophic and non-quasigeostrophic vertical motions for a model-simulated rapidly intensifying marine extratropical cyclone. *Monthly Weather Review*, 120(7):1108–1134.

Pfahl, S., O'Gorman, P. A., and Singh, M. S. (2015). Extratropical cyclones in idealized simulations of changed climates. *Journal of Climate*, 28(23):9373–9392.

Pirret, J. S., Knippertz, P., and Trzeciak, T. M. (2017). Drivers for the deepening of severe European windstorms and their impacts on forecast quality. *Quarterly Journal of the Royal Meteorological Society*, 143(702):309–320.

Pithan, F., Shepherd, T. G., Zappa, G., and Sandu, I. (2016). Climate model biases in jet streams, blocking and storm tracks resulting from missing orographic drag. *Geophysical Research Letters*, 43(13):7231–7240.

Räisänen, J. (1995). Factors affecting synoptic-scale vertical motions: a statistical study using a generalized omega equation. *Monthly Weather Review*, 123(8):2447–2460.

Räisänen, J. (1997). Height tendency diagnostics using a generalized omega equation, the vorticity equation, and a nonlinear balance equation. *Monthly Weather Review*, 125(7):1577–1597.

Ralph, F. M., Neiman, P. J., Wick, G. A., Gutman, S. I., Dettinger, M. D., Cayan, D. R., and White, A. B. (2006). Flooding on California's Russian River: Role of atmospheric rivers. *Geophysical Research Letters*, 33(13).

Roebber, P. J. and Schumann, M. R. (2011). Physical processes governing the rapid deepening tail of maritime cyclogenesis. *Monthly Weather Review*, 139(9):2776–2789.

Rolfson, D. M. and Smith, P. J. (1996). A composite diagnosis of synoptic-scale extratropical cyclone development over the United States. *Monthly Weather Review*, 124(6):1084–1099.

Rossby, C. (1939). Planetary flow patterns in the atmosphere. *Quarterly Journal of the Royal Meteorological Society*, 66:68.

Schultz, D. M., Bosart, L. F., Colle, B. A., Davies, H. C., Dearden, C., Keyser, D., Martius, O., Roebber, P. J., Steenburgh, W. J., Volkert, H., et al. (2019). Extratropical cyclones: a century of research on meteorology's centerpiece. *Meteorological Monographs*, 59:16–1.

Seiler, C. and Zwiers, F. W. (2016). How will climate change affect explosive cyclones in the extratropics of the Northern Hemisphere? *Climate Dynamics*, 46(11-12):3633–3644.

Sekioka, M. (1956). A hypothesis on complex of tropical and extratropical cyclones for typhoon in the middle latitudes. *Journal of the Meteorological Society of Japan. Ser. II*, 34(5):276–287.

Serreze, M., Barrett, A., Stroeve, J., Kindig, D., and Holland, M. (2009). The emergence of surface-based Arctic amplification. *The Cryosphere*, 3(1):11–19.

Shamarock, W., Klemp, J., Dudhia, J., Gill, D., Barker, D., Duda, M., Huang, X., Wang, W., and Powers, J. (2008). A description of the advanced research WRF version 3. *NCAR technical note NCAR/TN–475+STR*.

Stepanyuk, O., Räisänen, J., Sinclair, V. A., and Järvinen, H. (2017). Factors affecting atmospheric vertical motions as analyzed with a generalized omega equation and the OpenIFS model. *Tellus A: Dynamic Meteorology and Oceanography*, 69(1):1271563.

Stewart, S. R. (2018). Tropical cyclone report: Hurricane Ophelia, 9–15 October 2017. *National Hurricane Center*.

Stoelinga, M. T. (1996). A potential vorticity-based study of the role of diabatic heating and friction in a numerically simulated baroclinic cyclone. *Monthly Weather Review*, 124(5):849–874.

Thompson, D. W. and Solomon, S. (2005). Recent stratospheric climate trends as evidenced in radiosonde data: global structure and tropospheric linkages. *Journal of Climate*, 18(22):4785–4795.

Tierney, G., Posselt, D. J., and Booth, J. F. (2018). An examination of extratropical cyclone response to changes in baroclinicity and temperature in an idealized environment. *Climate Dynamics*, 51(9-10):3829–3846.

Tracton, M. S. (1973). The role of cumulus convection in the development of extratropical cyclones. *Monthly Weather Review*, 101(7):573–593.

Wernli, H., Dirren, S., Liniger, M. A., and Zillig, M. (2002). Dynamical aspects of the life cycle of the winter storm 'Lothar'(24–26 December 1999). *Quarterly Journal of the Royal Meteorological Society*, 128(580):405–429.

Wernli, H. and Schwierz, C. (2006). Surface cyclones in the ERA-40 dataset (1958–2001). Part I: novel identification method and global climatology. *Journal of the Atmospheric Sciences*, 63(10):2486–2507.

Willison, J., Robinson, W. A., and Lackmann, G. M. (2013). The importance of resolving mesoscale latent heating in the North Atlantic storm track. *Journal of the Atmospheric Sciences*, 70(7):2234–2250.

Willison, J., Robinson, W. A., and Lackmann, G. M. (2015). North Atlantic storm-track sensitivity to warming increases with model resolution. *Journal of Climate*, 28(11):4513–4524.

Yettella, V. and Kay, J. E. (2017). How will precipitation change in extratropical cyclones as the planet warms? Insights from a large initial condition climate model ensemble. *Climate Dynamics*, 49(5-6):1765–1781.

Yoshida, A. and Asuma, Y. (2004). Structures and environment of explosively developing extratropical cyclones in the northwestern Pacific region. *Monthly Weather Review*, 132(5):1121–1142.

Zappa, G., Shaffrey, L. C., and Hodges, K. I. (2013a). The ability of CMIP5 models to simulate North Atlantic extratropical cyclones. *Journal of Climate*, 26(15):5379–5396.

Zappa, G., Shaffrey, L. C., Hodges, K. I., Sansom, P. G., and Stephenson, D. B. (2013b). A multimodel assessment of future projections of North Atlantic and European extratropical cyclones in the CMIP5 climate models. *Journal of Climate*, 26(16):5846–5862.

Zwack, P. and Okossi, B. (1986). A new method for solving the quasi-geostrophic omega equation by incorporating surface pressure tendency data. *Monthly Weather Review*, 114(4):655–666.